Lithosphere

Two-stage development of the Paparoa Metamorphic Core Complex, West Coast, South Island, New Zealand: Hot continental extension precedes sea-floor spreading by ~25 m.y.

Daniel O. Schulte, Uwe Ring, Stuart N. Thomson, Johannes Glodny and Hamish Carrad

Lithosphere published online 2 April 2014;
doi: 10.1130/L348.1

Notes

Lithosphere, published online on 2 April 2014 as doi:10.1130/L348.1

Two-stage development of the Paparoa Metamorphic Core Complex, West Coast, South Island, New Zealand: Hot continental extension precedes sea-floor spreading by ~25 m.y.

Daniel O. Schulte[1], Uwe Ring[2], Stuart N. Thomson[3], Johannes Glodny[4], Hamish Carrad[5]
[1]INSTITUTE FOR APPLIED GEOSCIENCES, TECHNISCHE UNIVERSITÄT DARMSTADT, 64287 DARMSTADT, GERMANY
[2]DEPARTMENT OF GEOLOGICAL SCIENCES, STOCKHOLM UNIVERSITY, SE-106 91 STOCKHOLM, SWEDEN
[3]DEPARTMENT OF GEOSCIENCES, UNIVERSITY OF ARIZONA, TUCSON, ARIZONA 85721-0077, USA
[4]DEUTSCHES GEOFORSCHUNGSZENTRUM (GFZ), TELEGRAFENBERG, 14473 POTSDAM, GERMANY
[5]4 O'DEA STREET, CARLISLE 6101, PERTH, AUSTRALIA

ABSTRACT

The Paparoa Metamorphic Core Complex (PCC) developed in the mid-Cretaceous due to continental extension, which conditioned the crust for the eventual breakup of the Gondwana Pacific margin and formation of the Tasman Sea. The PCC has two detachment systems with opposite senses of shear: the top-to-the-NE Ohika Detachment in the north and the top-to-the-SW Pike Detachment in the south. Rb-Sr dating on mylonite shows that the Pike Detachment was active before 116.2 ± 5.9 Ma. It was the dominant detachment exhuming Cretaceous synextensional migmatites and was synchronous with the intrusion of the Buckland Granite, from which U-Pb zircon crystallization ages between 110.41 and 109.73 Ma were obtained. The ductile shear zone beneath the Pike Detachment records upper-amphibolite to lower-greenschist facies metamorphism and cataclastic deformation. Pronounced hydrothermal alteration at 108.91 ± 0.04 Ma is interpreted to be related to initial movement on the Ohika Detachment. The structural hinge separating top-to-the-SW from top-to-the-NE shearing has been located in the northern part of the PCC, also indicating that the Pike Detachment is the master detachment of the PCC. Fission-track data indicate a period of enhanced heat flow resulting in reset and partially reset apatite and zircon fission-track ages at ca. 75 Ma concurrent with the onset of sea-floor spreading in the Tasman Sea. Our data show that initial extension in the mid-Cretaceous proceeded under high-temperature conditions and preceded continental breakup by ~25 m.y.

LITHOSPHERE doi: 10.1130/L348.1

INTRODUCTION

Metamorphic core complexes can be precursors of continental breakup and result from extreme extension where the lower crust is dragged to the surface below large-scale extensional faults (Coney, 1980; Lavier et al., 1999; Lister and Davis, 1989). The thermal state of continental crust and its rheological structure control the variation between flow in the ductile lower crust and localized deformation in the brittle upper crust and explain the location and general architecture of core complexes (Gessner et al., 2007). A hot lithosphere with a weak lower crust facilitates lateral viscous flow across normal fault systems resulting in the formation of metamorphic core complexes (Block and Royden, 1990; Gessner et al., 2007). Bivergent core complexes (i.e., two oppositely dipping detachment faults on either side of the core complex) usually form in hot lithosphere (Gessner et al., 2007). Such hot lithosphere needs to cool down before it can break apart (Buck, 1991), leaving a time gap between initial extension and continental breakup. Detailed analyses of the structure, geometry and temporal evolution of a hot core complex can contribute to the understanding of the large-scale tectonic evolution of overheated lithosphere and the timing between continental extension and the onset of sea-floor spreading.

The Paparoa Metamorphic Core Complex (PCC) on the West Coast of the South Island of New Zealand is a bivergent core complex, characterized by the top-to-the-SW Pike Detachment at its southern end and the top-to-the-NE Ohika Detachment in the north (Tulloch and Kimbrough, 1989) (Fig. 1). Spell et al. (2000) proposed that extension initiated at the Ohika Detachment, but subsequently most of the extension was accommodated along the Pike Detachment. Critical in this regard is which detachment was synchronous with emplacement of the Buckland Granite, which in map view makes up a third of the exposed lower plate of the PCC and is exposed in the footwall of the Ohika Detachment (Nathan, 1978; Tulloch and Kimbrough, 1989). Furthermore, Spell et al. (2000) suggest continuous cooling of the metamorphic core over ~20 m.y., which was rapid at first and slowed down after 90 Ma.

The results of this paper show that the top-to-the-SW Pike Detachment accommodated most of the extension, became active first, and was synchronous with the emplacement of the Buckland Granite. The hinge of the two detachment systems can be located between Mount Kelvin and Buckland Peaks in the northern part of the PCC close to the Ohika Detachment. The Ohika Detachment is interpreted as a late minor feature of the core complex structure accommodating the final exhumation of the Buckland Granite. Fission-track ages reveal a complicated history of burial, reheating, and exhumation after the PCC's initial exhumation, which can be related to events associated with the Late Cretaceous period of continental breakup. Our work shows that the extension of hot and weak magmatic arc lithosphere is a prolonged event. The West Coast of New Zealand extended read-

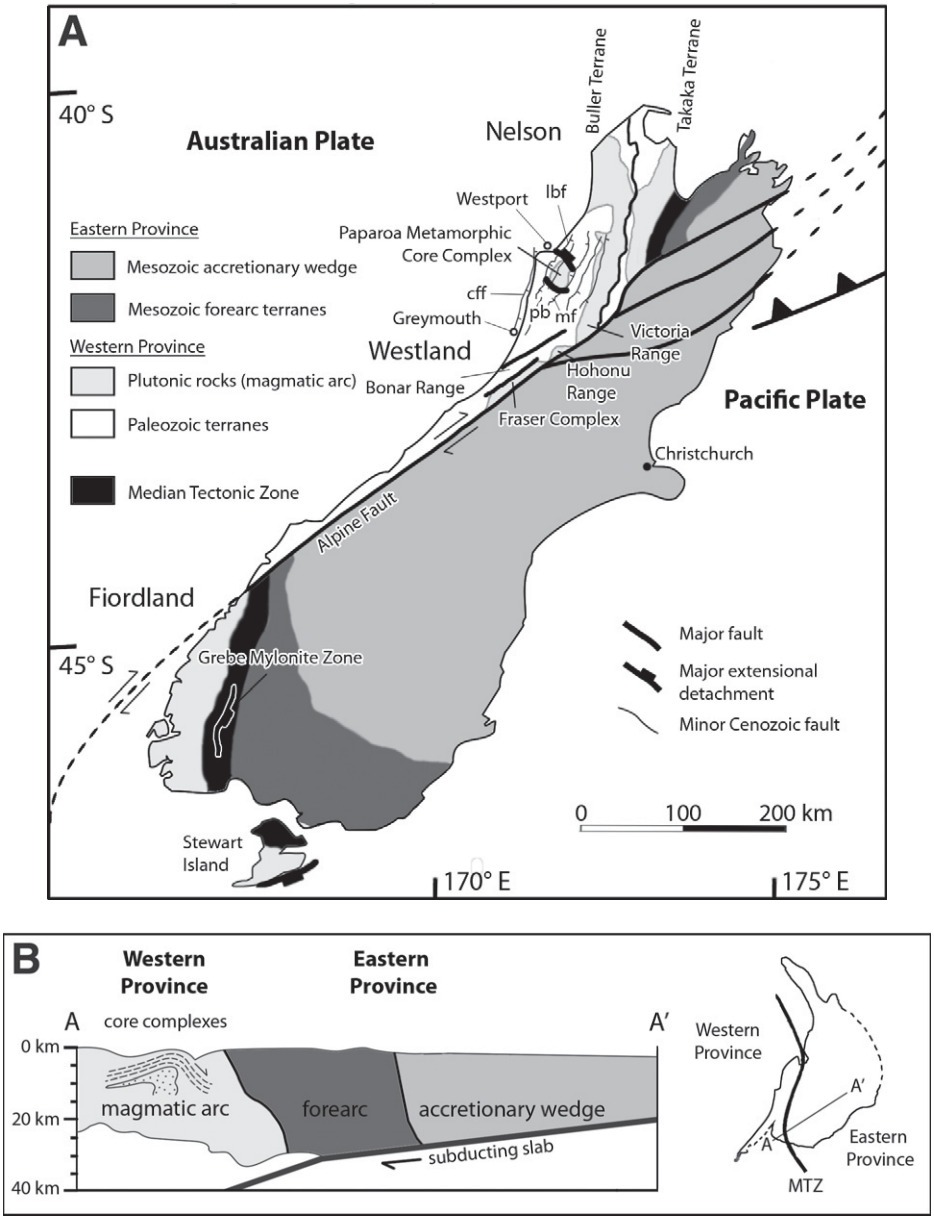

Figure 1. Overview of the Mesozoic terranes of the South Island of New Zealand (A) and a schematic cross section of pre-Alpine Fault Zealandia (B) (simplified after Mortimer et al., 2002). Shown are major Cretaceous extensional detachments in Paparoa Range, Fiordland, and on Stewart Island (after Gibson et al., 1988; Ireland and Gibson, 1998; Kula et al., 2007; Tulloch and Kimbrough, 1989). Also shown are major Late Cenozoic faults related to the Kaikoura orogeny and minor Cenozoic faults facilitating the pop-up of the Paparoa Metamorphic Core Complex. Abbreviations: pb—Paparoa Basin; cff—Cape Foulwind Fault; lbf—Lower Buller Fault; mf—Maimai Fault (after Ghisetti and Sibson, 2006); MTZ—Median Tectonic Zone (after Bradshaw, 1993; Mortimer et al., 1999).

ily in the mid-Cretaceous and needed ~25 m.y. to cool down enough to break apart.

GEOLOGY

New Zealand

The basement of the South Island of New Zealand consists of several Paleozoic and Mesozoic terranes, which are divided into the Eastern Province and the Western Province along a tectonic boundary called the Median Tectonic Zone (Bradshaw, 1989, 1993). The provinces are transected and dextrally offset by ~480 km along the Miocene to Recent Alpine Fault (Fig. 1A).

The Eastern Province consists of volcanogenic material and accretionary complexes that formed along the convergent Pacific-Gondwana plate boundary (Bradshaw, 1989) until 115–108 Ma (Adams et al., 2009; Cawood et al., 1999) (Fig. 1B). In contrast, the Western Province represents a fragment of the eastern continental margin of Gondwana (Bradshaw, 1993). It consists of low-grade metasedimentary rocks grouped into the Buller and Takaka Terranes. The rocks of the Western Province were intruded by several NE-SW–oriented batholiths and plutons (Muir et al., 1994). Based on their age and chemistry, Tulloch (1988) defined three suites: S-type granitoids of Devonian to Carboniferous age are confined to the Buller Terrane and belong to the Karamea Suite. The Separation Point Suite comprises Cretaceous I-type granitoids and occurs in both terranes. Cretaceous granitoids of transitional I/S-type signature characterize the Rahu Suite. The Rahu Suite is restricted to the Buller Terrane. Granites of this suite make up parts of the PCC lower plate, namely the orthogneissic parts of the Charleston Metamorphic Group and the Buckland Granite (Muir et al., 1994; Tulloch and Kimbrough, 1989; White, 1994). The latter is of particular importance for the development of the PCC.

In the mid-Cretaceous, convergent margin tectonics in New Zealand came to an end and lithospheric extension set in (Bradshaw, 1989). The cause of lithospheric extension is not clear, as is the question whether extension commenced during or after subduction. The latter lasted until ca. 110–100 Ma and was diachronous along the margin (Mortimer et al., 2006). Extension preceding the breakup of Gondwana caused the development of detachment faults and core complexes, which can be found in Stewart Island, Fiordland and Westland (Fig. 1, Gibson et al., 1988; Ireland and Gibson, 1998; Kula et al., 2007; Tulloch and Kimbrough, 1989). The core complexes formed along the magmatic arc of the subduction system, which shows that the thermal structure of the subduction system controlled the localization of extensional deformation (Waight et al., 1998) (Fig. 1B).

The unroofing of the metamorphic cores led to the deposition of breccias of basement-derived rocks in adjacently developing NW-trending half-graben (Laird and Bradshaw, 2004). The eventual separation of Australia and New Zealand at ca. 84 Ma (Gaina et al., 1998) was accompanied by alkaline volcanism (Laird, 1994). NW-striking swarms of lamprophyric dikes in Nelson have been dated as 86–80 Ma (Adams and Nathan, 1978; recalculated by Laird, 1994). The inception of seafloor spreading also marks the beginning of the formation of the Paparoa Basin near Greymouth and the deposition of the Paparoa Coal Measures in a series of half graben (Laird, 1994). Bassett et al. (2006) showed that the content of metamorphic detritus increases in

the upper parts of the basin fill. Sedimentation lasted until the Late Paleocene and was followed by emergence and erosion, which resulted in peneplanation of the West Coast region. Subsequently the Brunner Coal Measures were deposited as a consequence of an Eocene transgression (Bassett et al., 2006; Seward, 1989).

During the late Cenozoic Kaikoura Orogeny the Australian and Pacific Plates collided resulting in the formation of the Southern Alps and shaping the overall architecture and topography of the New Zealand continent (Kingma, 1959). The main plate boundary structure in the Southern Alps is the Alpine Fault (Wellman, 1955). West of the Alpine Fault a number of NNE-striking reverse faults are associated with local foreland basins and pop-up structures in the footwall of the Alpine Fault (Fig. 1). One such pop-up structure is the Paparoa Range, which is bounded by the E-dipping Lower Buller reverse fault on its western side and the associated W-dipping Inangahua and Maimai reverse faults in the east (Ghisetti and Sibson, 2006). Within the Paparoa Range a few minor NNE-striking reverse faults occur (Fig. 2A). It is this late Cenozoic pop-up that (re)exposed the PCC.

West of the Paparoa Range the offshore E-dipping Cape Foulwind Fault lifted up the coastal plain between Westport and Greymouth (Figs. 2A, 2B). As a consequence of this uplift, the lower plate of the PCC is also exposed along the coastline (Laird, 1968; Seward and White, 1992). Vitrinite reflectance data show that the coastal part of the PCC was buried distinctly less in the early Cenozoic than the Paparoa Range itself (Kamp et al., 1999; Nathan et al., 1986; Suggate, 1959).

The Paparoa Metamorphic Core Complex

In the Paparoa Range, low-grade metasedimentary rocks and mid-Cretaceous graben-fill deposits are tectonically juxtaposed against high-grade metamorphic rocks. Tulloch and Kimbrough (1989) were the first to explain this by suggesting a bivergent metamorphic core complex origin of the Paparoa Range. Accordingly, the low-grade metasediments of the early Paleozoic Greenland Group and the mid-Cretaceous terrestrial conglomerates of the Pororari Group comprise the upper plate of the core complex, while gneisses of the Charleston Metamorphic Group (CMG, i.e., paragneiss and orthogneiss as defined by White, 1994), Late Paleozoic granitoids (Windy Point and Cape Foulwind Granites, Muir et al., 1994), and the Cretaceous Buckland Granite with associated intrusions of similar age, constitute the lower plate (Fig. 2C). The faults separating these units are low-angle normal faults (detachments). Two detachment faults have been recognized: the top-to-the-SW Pike Detachment in the south and the top-to-the-NE Ohika Detachment in the north (Tulloch and Kimbrough, 1989).

Lower Plate. The lower plate of the PCC is chiefly made up of the CMG (Nathan, 1978; Tulloch and Kimbrough, 1989; White, 1994). The CMG is a heterogeneous unit consisting of para- and orthogneiss (Sagar and Palin, 2011; White, 1994). In the southern part of the PCC, White (1994) found increasing metamorphic conditions toward the Pike Detachment and mapped the isograd muscovite + quartz = sillimanite + potassium feldspar + fluid (Fig. 2A). Geothermobarometric calculations for sillimanite and almandine bearing paragneiss provide P-T conditions of 600 ± 50 °C and 4 ± 1 kbar (White, 1994). The occurrence of migmatite and the lack of wollastonite farther south indicate temperatures between ~650 and 700 °C (White, 1994). Deformation of the CMG rocks in the southern part of the PCC resulted in the local formation of upper amphibolite facies ultramylonites south of Charleston. Sericite in basement breccia below the Pike Detachment yield K/Ar ages of 84.9 ± 1.3 Ma and 86.0 ± 1.0 Ma (Tulloch and Palmer, 1990).

In the central part of the lower plate near Charleston, zircons of the CMG orthogneiss yield two significantly different Cretaceous U-Pb age populations at 118 ± 2 Ma and 107 ± 2 Ma (Sagar and Palin, 2011) (see Fig. 3 for compilation of ages). The older age was obtained from oscillatory-zoned zircon sectors, while the younger age was obtained from featureless overgrowth rims typical of metamorphic zircon. The ages were attributed to the emplacement of the granite protolith of the Charleston Orthogneiss at 118 ± 2 Ma and a subsequent amphibolite facies metamorphic overprint at 107 ± 2 Ma (Sagar and Palin, 2011). The protolith of the CMG paragneiss is ca. 360 million years old (U-Th-Pb monazite age; Ireland and Gibson, 1998). A post-metamorphic granite dike near Charleston crosscuts the penetrative foliation. It has itself a weak tectonic foliation, which parallels that in the host rock, indicating that the intrusion of the dike at 105 ± 2 Ma (U-Pb zircon age) was late-tectonic (Sagar and Palin, 2011).

The northern part of the PCC consists mainly of plutonic rocks. The Windy Point Granite and the Cape Foulwind Granite beneath the Ohika Detachment (Fig. 2A) have U-Pb zircon crystallization ages of 328.6 ± 4.1 Ma and 327.3 ± 6.2 Ma respectively (Muir et al., 1994). The Buckland Granite makes up most of the northern third of the PCC and intruded at a depth of 10–18 km (White, 1994). One sample of Buckland Granite yielded a U-Pb zircon crystallization age of 109.6 ± 1.7 Ma (Muir et al., 1994). U-Pb TIMS dating of four samples of Buckland Granite by Buchwaldt et al. (2011) yielded more precise zircon ages ranging between 110.24 ± 0.17 Ma and 109.86 ± 0.13 Ma. The co-magmatic Steele Granite yields an $^{40}Ar/^{39}Ar$ hornblende age of 110.7 ± 1.1 Ma (Spell et al., 2000).

Strongly hydrothermally altered zircon from an outcrop of ultracataclastically deformed Buckland Granite within the Ohika detachment zone yields an U-Pb age of 108.91 ± 0.04 Ma (Buchwaldt et al., 2011), which is significantly younger than the crystallization age of the Buckland Granite. Sericite of hydrothermally altered basement breccia below the Ohika Detachment yielded K/Ar ages of 98.3 ± 1.4 Ma and 97 ± 1.4 Ma, which are markedly older than the K/Ar sericite ages of altered basement breccia obtained for the Pike Detachment (Tulloch and Palmer, 1990).

Upper Plate. Adjacent to the two detachments on either side of the PCC, WNW-ESE–oriented grabens have been filled with the mid-Cretaceous Pororari Group. The Pororari Group consists of overlapping alluvial and lacustrine fans (Laird, 1995). The sedimentary rocks rest directly above the Pike Detachment and the eastern Ohika Detachment (Tulloch and Kimbrough, 1989). In the western portion of the Ohika Detachment, the early Paleozoic Greenland Group underlies the Pororari Group sedimentary rocks (Tulloch and Kimbrough, 1989). Internal normal faulting and domino-style rotation toward the detachment fault within the Pororari Group indicate that extensional deformation was active during deposition of the Pororari Group (Tulloch and Kimbrough, 1989).

The sedimentary rocks of the Pororari Group at the northern and southern end of the PCC differ markedly. In the south, the Buckland Granite is the predominant source for fanglomerates above the Pike Detachment. Granitic cobbles are abundant in the Hawks Crag Breccia. Some of the clasts of Buckland Granite, which are up to 30–40 cm in size, show evidence of ductile deformation (Tulloch and Palmer, 1990). At Bullock Creek, the granitic cobbles yielded K/Ar muscovite ages of 114.6 ± 1.2 Ma, 113.4 ± 1.6 Ma, 106.1 ± 1.0 Ma and 107.7 ± 1.8 Ma (Tulloch and Palmer, 1990), which overlap with or appear to be slightly older than the precise U-Pb zircon crystallization ages of Buchwaldt et al. (2011) for the Buckland Granite. Deposits of the Pororari Group at the southern end of the PCC yielded Urutawan to Motuan (i.e., 108.4–103.3 Ma and 103.3–100.2 Ma respectively, Cooper, 2004; timescale after Hollis et al., 2010) palynological ages (Raine, 1984) that are significantly older than the palynological ages for the Pororari Group at the northern end of the PCC.

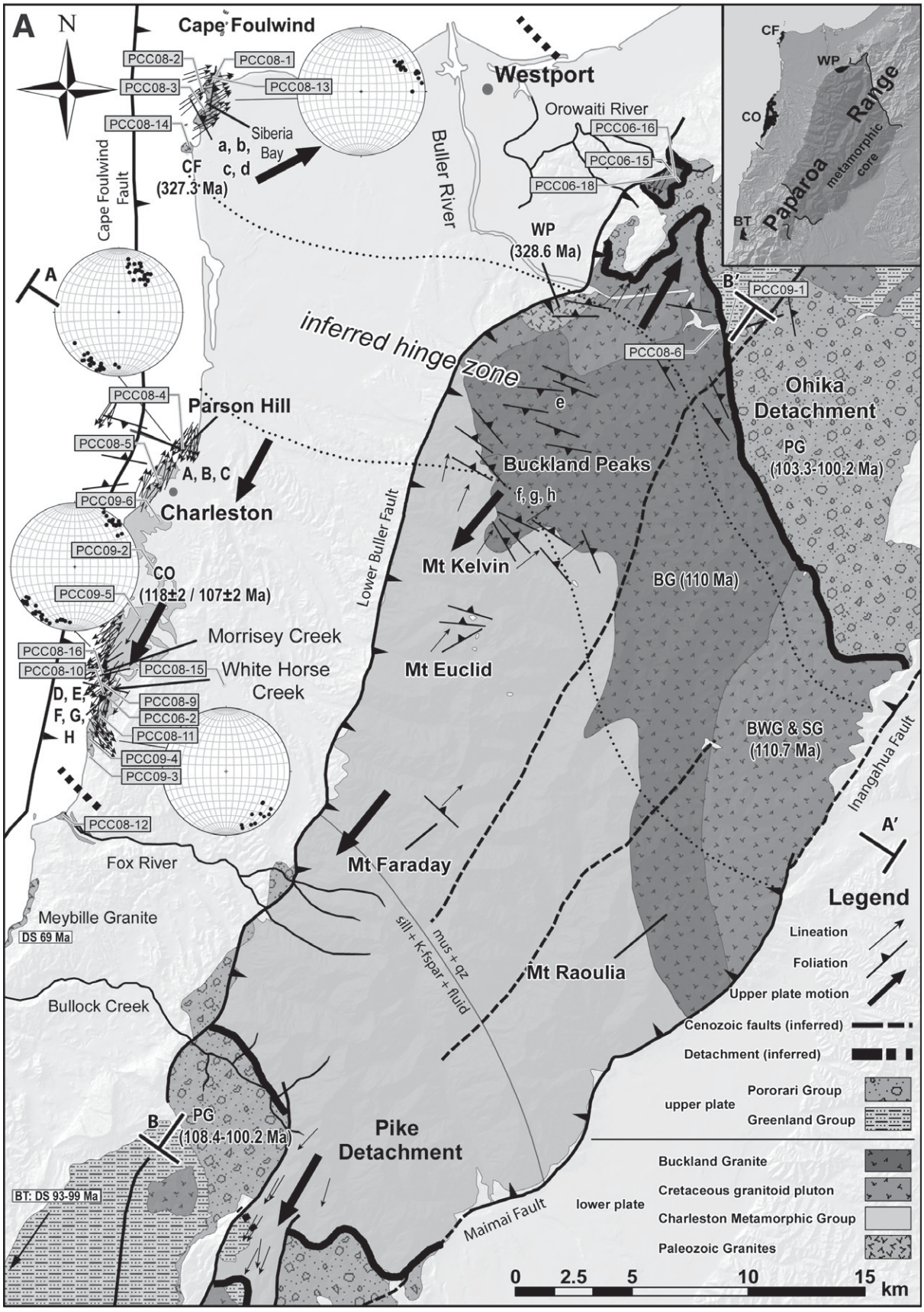

Figure 2. (*Continued on following page.*)

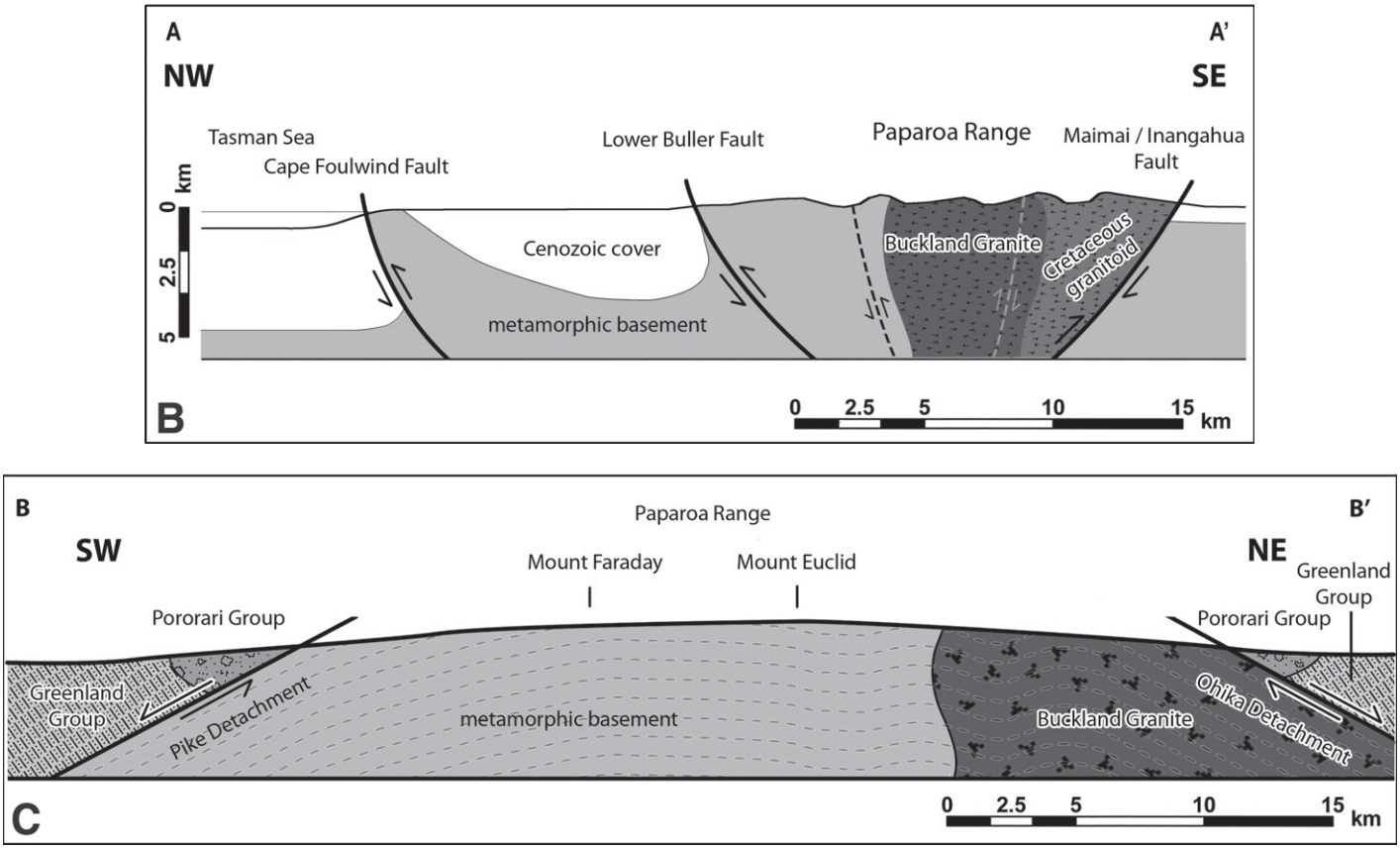

Figure 2. Generalized geological map of the Paparoa Metamorphic Core Complex (A) with schematic cross sections across (B) and along (C) the Paparoa Range. Dashed lines in lower plate in (C) represent overall foliation geometry. The geology is after Tulloch and Kimbrough (1989) and Rattenbury et al. (1998); faults and inferred faults according to Ghisetti and Sibson (2006). Note that the present exhumation level is due to erosion since the inception of the Paparoa Range pop-up. The lower hemisphere equal area projections (Allmendinger et al., 2013; Cardozo and Allmendinger, 2013) display the distribution of lineations measured at Cape Foulwind, Parson Hill and Charleston, and the southern coastal section. The two dotted lines in the northern Paparoa Metamorphic Core Complex (PCC) show the inferred structural hinge zone; the thin gray line in the southern PCC shows the sillimanite + potassium feldspar isograd mapped by White (1994). Abbreviations: a–h—locations of photos in Figure 4; A–H—locations of photos in Figure 5; PCCxx-xx—locations of Rb-Sr and fission-track samples; DSxx-xx—fission-track ages by Seward (1989); BG—Buckland Granite; BWG—Blackwater Granite; SG—Steele Granite; BT—Barrytown Granite; CF—Cape Foulwind Granite; CO—Charleston Orthogneiss; WP—Windy Point Granite; PG—Pororari Group.

The base of the Pororari Group in the lower Buller Gorge in the north mainly contains small clasts, generally less than 10 cm in size, of Greenland Group sediments and undeformed Paleozoic granites. Cobbles of Buckland Granite, which are rare in the Hawks Crag Breccia, provided K/Ar muscovite ages of 112.4 ± 1.6 Ma, 114.1 ± 1.6 Ma and 111.3 ± 1.4 Ma (Tulloch and Palmer, 1990). U-Pb zircon ages from the Stitts Tuff near the base of the Pororai Group are 101 ± 2 Ma and 102 ± 3 Ma (Muir et al., 1997). These ages are in agreement with Motuan (103.3–100.2 Ma) palynological ages (Raine, 1984).

Current tectonic model for PCC. Based on $^{40}Ar/^{39}Ar$ ages of white mica, hornblende and feldspar, Spell et al. (2000) proposed rapid footwall cooling from temperatures of 500 °C to 170 °C at rates up to ~110 °C Ma^{-1} between ca. 110 and 90 Ma followed by continuous and slow cooling (~5 °C Ma^{-1}) of the PCC between 90 and 80 Ma. Spell et al. (2000) proposed that the Ohika Detachment is older than the Pike Detachment and that the intrusion of the Buckland Granite locked-up the Ohika Detachment. The exhumation of the Buckland Granite and the CMG was chiefly accommodated by the Pike Detachment. Based on their $^{40}Ar/^{39}Ar$ ages, and K/Ar-muscovite ages of Tulloch and Kimbrough (1989), Spell et al. (2000, their fig. 10) calculated a slip rate of 4.4 km Ma^{-1} at 102–93 Ma for the Pike Detachment. The authors suggested that the Pororari Group at the southern end of the PCC was deposited adjacent to the Buckland Granite and subsequently displaced along to Pike Detachment to its present position. If the Ohika Detachment is indeed older than the Pike Detachment and synchronous with the emplacement of the Buckland Granite, then the Buckland Granite should have been transported and exhumed in a southerly direction in the footwall of the Ohika Detachment. We revisited ductile deformation features along the two PCC detachments and studied the temperature and deformation history using structural field data, fission-track thermochronology and Rb-Sr dating of mylonite to put tighter constraints on the history of the PCC.

METHODS

Fission-Track Thermochronology

Fission tracks (FT) in apatite and zircon can provide important information on the low-temperature (<300 °C) cooling history of rocks (e.g., Fleischer et al., 1975) as they anneal at different temperatures. At temperatures above 60 °C, apatite of a typical Durango standard composition begins to anneal over geologic times-

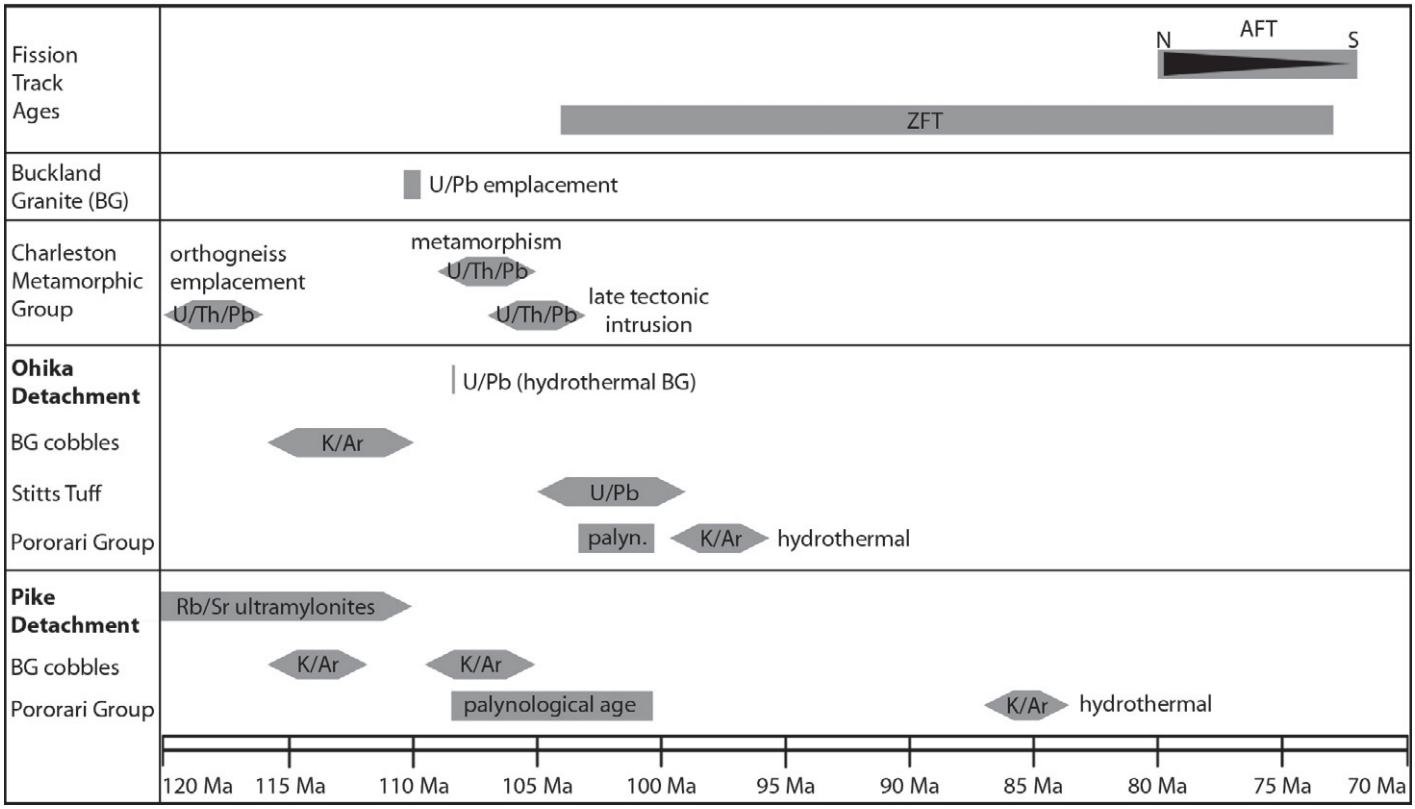

Figure 3. Compilation of age data from the Paparoa Metamorphic Core Complex, tapering bars include age uncertainties, see text for discussion.

cales: between 100 °C and 120 °C the tracks are completely annealed and the FT age is entirely reset (Green et al., 1989; Ketcham et al., 1999). This temperature range (60–120 °C) is called the apatite FT partial annealing zone. The closure temperature for the retention of FT depends on the cooling rate (Seward, 1989); pressure has no significant effect on the annealing (Naeser and Faul, 1969). For moderate cooling rates of 10–40 °C Ma^{-1} a closure temperature of 110 ± 10 °C can be assumed (Ketcham et al., 1999; Reiners and Brandon, 2006). Zircon retains FT to higher temperatures. For pristine grains, annealing over geological time starts upon heating at ~250 ± 20 °C and total resetting is reached above 310 ± 10 °C (Tagami et al., 1998). As these temperatures are lower in zircons that are strongly affected by radiation damage (Brandon et al., 1998; Rahn et al., 2004), this translates to a closure temperature for the retention of fission tracks of ~240 ± 20 °C in zircon of average radiation damage at moderate cooling rates of around 10 °C Myr^{-1} (Bernet, 2009).

Samples for FT analysis were taken mainly on the coastline between Cape Foulwind and the Fox River mouth (Fig. 2). Seward (1989) proposed that the coastal strip experienced continuous exhumation and cooling from the mid-Cretaceous to the early Eocene. The methodology for sample processing as described by Thomson and Ring (2006) was applied. The samples were irradiated at the Oregon State University Triga Reactor, Corvallis, Oregon, USA. IRMM540R and IRMM541 dosimeter glasses were used to monitor neutron fluence. Age calculations are based on zeta calibration factors (Hurford and Green, 1983) 368.1 ± 14.9 (IRMM540R apatite) and 121.1 ± 3.5 (IRMM541 zircon). Obtained central ages (Galbraith and Laslett, 1993) were calculated following the IUGS recommended Zeta-calibration approach of Hurford and Green (1983) (Tables 1 and 2). The probability that the single grain FT ages determined from a single sample belong to a single age population is assessed using a χ^2-test and the age dispersion (Galbraith and Laslett, 1993). If a central age fails the test (χ^2 probability of <5%, or age dispersion >10%) the single grains ages from that sample represent a mixed age population. For the zircon FT data (Table 2) we deconvoluted the youngest age population (P1) using the mixture modeling algorithm of Sambridge and Compston (1994) contained in the Isoplot/Ex program (Ludwig, 2012). A new central age was then calculated for each grain age population identified (Table 2).

Rb-Sr Geochronology

For direct dating of ductile deformation in an ultramylonite sample from beneath the Pike detachment we used the Rb-Sr internal mineral isochron approach on bulk mineral separates (e.g., Glodny et al., 2008a). From the sample (~50 g in total) we separated feldspar, three different grain-size fractions of white mica, and fragments of the homogeneous fine-grained ultramylonitic matrix. The Rb-Sr isotope system of the age-constraining white mica is thermally stable to temperatures higher than 600 °C for geologic timescales (Glodny et al., 2008a) but may be fully reset by dynamic recrystallization at temperatures as low as 350 °C (Müller et al., 1999). Penetrative synkinematic recrystallization in mylonites is usually accompanied by isotopic re-equilibration (Cliff and Meffan-Main, 2003; Müller et al., 1999; Müller et al., 2000). Therefore, white mica-based Rb-Sr mineral isochron data from penetratively deformed rocks can generally be used to date the waning stages of mylonitic deformation. White mica was analyzed in different grain-size fractions to detect possible Sr isotope inhomogeneities resulting from (1) isotopic inheritance; (2) long-term or incomplete dynamic recrystallization; (3) dif-

TABLE 1. PAPAROA APATITE FISSION-TRACK DATA

Sample no.	No. of crystals	Track density (x 10^6 tr cm^{-2})			Age dispersion	Central age (Ma) (±1σ)	Apatite mean track length (μm ± 1 s.e.) (no. of tracks)	Standard deviation (μm)
		ρ_s (N_s)	ρ_i (N_i)	ρ_d (N_d)	($P\chi^2$)			
PCC06-15	20	0.1568 (94)	1.638 (982)	1.304 (4174)	0.06% 89.0%	**22.9 ± 2.7**	-	-
PCC06-16	20	0.3842 (194)	2.727 (1377)	1.297 (4152)	50.2% <0.01%	**33.6 ± 4.9 (mixed age)**	-	-
PCC06-17	4	0.4893 (62)	3.354 (425)	1.290 (4130)	0.6% 32.5%	**34.5 ± 4.9 (mixed age?)**	-	-
PCC06-18	20	0.7348 (324)	6.307 (2781)	1.284 (4107)	46.6% <0.01%	**29.1 ± 3.7 (mixed age)**	**14.39 ± 0.11 (84)**	**0.98**
PCC08-1	20	2.226 (980)	6.734 (2965)	1.277 (4085)	0.04% 87%	**77.2 ± 4.4**	**13.35 ± 0.12 (100)**	**1.20**
PCC08-2	20	1.698 (890)	4.909 (2573)	1.270 (4063)	0.06% 88%	**80.4 ± 4.7**	**13.56 ± 0.13 (100)**	**1.26**
PCC08-3	20	2.720 (1055)	8.310 (3223)	1.263 (4041)	0.01% 93.8%	**75.7 ± 4.2**	**13.64 ± 0.12 (100)**	**1.19**
PCC08-4	20	0.6869 (506)	2.135 (1573)	1.256 (4019)	<0.01% >99%	**73.9 ± 5.0**	**13.96 ± 0.13 (100)**	**1.27**
PCC08-5	20	0.6521 (429)	1.911 (1257)	1.249 (3996)	<0.01% >99%	**78.0 ± 5.5**	**13.76 ± 0.13 (100)**	**1.31**
PCC08-6	20	0.2341 (166)	2.230 (1581)	1.242 (3974)	45.2% 0.02%	**23.7 ± 3.3 (mixed age)**	-	-
PCC08-9	20	0.8772 (503)	2.651 (1520)	1.235 (3952)	<0.01% 98.3%	**74.8 ± 5.0**	**14.22 ± 0.15 (51)**	**1.05**
PCC08-10	2	0.8523 (24)	2.663 (75)	1.228 (3930)	<0.01% 70.4%	**71.9 ± 17.2**	-	-
PCC08-11	20	0.6678 (303)	2.065 (937)	1.221 (3907)	<0.01% >99%	**72.3 ± 5.7**	**13.11 ± 0.14 (100)**	**1.37**
PCC08-12	20	1.271 (581)	3.869 (1768)	1.214 (3885)	<0.01% >99%	**73.0 ± 4.7**	**13.61 ± 0.12 (100)**	**1.20**
PCC08-13	20	1.474 (666)	4.125 (1864)	1.207 (3863)	<0.01% 97.9%	**78.9 ± 5.0**	**13.58 ± 0.12 (100)**	**1.20**
PCC08-14	20	0.9685 (344)	2.880 (1023)	1.200 (3841)	<0.01% >99%	**73.8 ± 5.6**	**13.42 ± 0.11 (100)**	**1.12**
PCC08-15	20	1.177 (656)	3.450 (1923)	1.193 (3819)	<0.01% >99%	**74.5 ± 4.7**	**13.18 ± 0.15 (100)**	**1.46**
PCC08-16	20	0.6607 (392)	1.922 (1140)	1.186 (3796)	<0.01% >99%	**74.6 ± 5.5**	**13.54 ± 0.11 (100)**	**1.06**

(i). Analyses by external detector method using 0.5 for the $4\pi/2\pi$ geometry correction factor.
(ii). Ages calculated using dosimeter glass: IRMM540R with ζ_{540R} = 368.1 ± 14.9 (apatite).
(iii). $P\chi^2$ is the probability of obtaining a χ^2 value for v degrees of freedom where v = no. of crystals −1.

fusional Sr redistribution; and (4) alteration processes. This approach ensures control on the possible presence of unequilibrated, pre-deformational white mica relics (Müller et al., 1999).

A detailed description of mineral processing and of the Rb-Sr analytical procedure is outlined in Glodny et al. (2008a). Isotopic measurements for Rb and Sr were carried out on a VG Sector 54 multicollector thermal ionization mass spectrometer (GFZ Potsdam). The value obtained for $^{87}Sr/^{86}Sr$ of the NBS standard SRM987 during analytical work was 0.710263 ± 0.000010 (n = 16). Isochron parameters were calculated using the Isoplot/Ex program (Ludwig, 2012). Decay constants are those recommended by Steiger and Jäger (1977). Standard errors of ± 0.005% for $^{87}Sr/^{86}Sr$ ratios and of ± 1.5% for Rb-Sr ratios, as derived from replicate analyses of spiked white mica samples, were applied in isochron age calculations.

DEFORMATION

Most of the exposed basement rocks in the PCC show evidence of ductile deformation. Deformation was heterogeneous due to compositional differences and availability of fluids during core complex formation. In general, there is a pronounced increase in brittle deformation and associated hydrothermal alteration toward the detachments. Mylonites and ultramylonites are developed in distinct layers below zones of brittle deformation. Shear-sense indicators in cataclasites, mylonites and ultramylonites below the Pike Detachment show top-to-the-SW movement, whereas deformed rocks in the footwall of the Ohika Detachment show a top-to-the-NE sense of shear (Fig. 2) (see also Tulloch and Kimbrough, 1989). Bedding in sedimentary rocks in NW oriented basins in the upper plates adjacent to the detachment faults dips back into the core complex, suggesting that SW-dipping normal faults in the south and NE-dipping normal faults in the north controlled basin architecture (Laird, 1994). This collective evidence strongly suggests that footwall deformation was related to mid-Cretaceous mid-crustal continental extension (Tulloch and Kimbrough, 1989) preceding the opening of the Tasman Sea. Late Cretaceous lamprophyre dikes associated with initial sea-floor spreading in the Tasman Sea are orientated perpendicular to the NE-SW extension direction (Tulloch and Kimbrough, 1989).

We describe the heterogeneous deformation along a NE-SW profile to show the differences in deformation in the footwalls of both detachments and to infer the hinge zone where top-to-the-NE shear changes to top-to-the-SW shear.

Footwall of Ohika Detachment

Deformation at the northern end of the PCC displays ductile structures in Siberia Bay (Fig. 2). There, the Cape Foulwind Granite has a strong foliation expressed by recrystallized quartz and biotite and large oligoclase porphyroclasts aligned parallel to the foliation (Fig. 4A). Oligoclase is not recrystallized (Fig. 4B). On the foliation a well-developed NE-trending stretching lineation occurs. Bookshelf structures in feldspar, chlorite-filled shear bands and mantled porphyroclasts provide a top-to-the-NE shear-sense (Fig. 4A and 4C). North of Siberia Bay toward the detachment fault deformation intensity becomes weaker grading into undeformed Cape Foulwind Granite that is unconformably overlain by Cenozoic sediments at the cape.

In the lower Buller Gorge, the Buckland Granite makes up the footwall of the Ohika Detachment. In the gorge, the granite is undeformed or mildly deformed with a weak NE-trending stretching lineation on a spaced foliation. The stretching lineation is mainly expressed by aligned and recrystallized quartz. North of the Buller River and in the east near the Ohika Detachment, the Buckland Granite shows a pronounced cataclastic overprint. Directly at the detachment in a road ditch along State Highway 6, the granite is extremely hydrothermally altered and displays pronounced cataclastic deformation that grades into a few centimeters thick zone of blackish ultracataclasite. All mineral grains are comminuted, formerly larger potassium feldspars are shattered aggregates of smaller angular grains and aligned chlorite and mica constitute a foliation (Fig. 4D). In the Orowaiti River west

TABLE 2. PAPAROA ZIRCON FISSION-TRACK DATA

Sample no.	No. of grains counted	Track density (x 10^6 tr cm^{-2}) ρ_s (N_s)	ρ_i (N_i)	ρ_d (N_d)	Age dispersion ($P\chi^2$)	Central age (Ma) (±2σ)	Population 1 Age (Ma) (±2σ) (No. of grains)	Population 2 Age (Ma) (±2σ) (No. of grains)
PCC06-15	20	8.618 (2118)	2.824 (694)	0.5071 (3246)	27.5% <0.01%	**84.1 ± 14.2 (mixed age)**	73.3 ± 8.8 (17)	180.5 ± 36.7 (3)
PCC06-16	20	7.430 (2059)	3.002 (832)	0.5053 (3234)	<0.01% (97.1%)	**75.3 ± 8.0**	n/a	n/a
PCC06-18	20	7.118 (1517)	2.557 (545)	0.5035 (3223)	<0.01% (97.3%)	**84.3 ± 10.2**	n/a	n/a
PCC08-1	20	17.06 (4423)	3.904 (1012)	0.5017 (3211)	29.0% <0.01%	**125.5 ± 20.4 (mixed age)**	102.8 ± 11.0 (14)	205.1 ± 47.0 (6)
PCC08-2	6	8.878 (534)	3.059 (184)	0.4999 (3199)	<0.01% (82.2%)	**87.3 ± 16.0**	n/a	n/a
PCC08-3	20	10.98 (3072)	2.621 (733)	0.4981 (3188)	21.2% (<0.01%)	**122.7 ± 17.2 (mixed age)**	97.8 ± 12.7 (11)	163.4 ± 23.2 (9)
PCC08-4	20	12.70 (2617)	3.931 (810)	0.4963 (3176)	16.3% (1.1%)	**94.6 ± 12.2 (mixed age)**	91.3 ± 9.8 (19)	208.7 ± 76.7 (1)
PCC08-5	20	9.093 (2031)	2.852 (637)	0.4945 (3165)	<0.01% (98.8%)	**94.8 ± 10.8**	n/a	n/a
PCC08-6	17	10.40 (2011)	3.415 (660)	0.4927 (3153)	<0.01% (99.9%)	**90.3 ± 10.2**	n/a	n/a
PCC08-9	20	14.49 (3208)	3.265 (723)	0.4909 (3141)	29.3% (<0.01%)	**118.7 ± 20.4 (mixed age)**	104.2 ± 12.4 (16)	214.0 ± 89.8 (4)
PCC08-10	7	4.801 (467)	1.717 (167)	0.4890 (3130)	<0.01% (99.8%)	**82.3 ± 15.8**	n/a	n/a
PCC08-11	20	11.83 (2672)	3.882 (877)	0.4872 (3118)	0.70% (55.7%)	**89.3 ± 9.2**	n/a	n/a
PCC08-12	20	7.976 (1996)	2.717 (680)	0.4854 (3107)	<0.01% (99.6%)	**85.7 ± 9.6**	n/a	n/a
PCC08-13	20	9.577 (2464)	2.865 (737)	0.4836 (3095)	0.88% (86.2%)	**97.2 ± 10.6**	n/a	n/a
PCC08-14	20	5.659 (2137)	1.833 (692)	0.4818 (3084)	<0.01% (98.6%)	**89.5 ± 10.0**	n/a	n/a
PCC08-16	20	13.89 (3671)	4.975 (1315)	0.4800 (3072)	0.15% (77.6%)	**80.6 ± 7.6**	n/a	n/a
PCC09-02	20	12.15 (4550)	4.610 (1726)	0.4782 (3060)	0.08% (94.2%)	**75.9 ± 6.8**	n/a	n/a
PCC09-03	2	12.38 (206)	4.327 (72)	0.4764 (3049)	<0.01% (92.0%)	**82.0 ± 23.2**	n/a	n/a
PCC09-04	1	11.94 (191)	4.625 (74)	0.4746 (3037)	n/a	**74.3 ± 20.8**	n/a	n/a
PCC09-05	20	11.72 (3121)	4.342 (1156)	0.4728 (3026)	<0.01% (94.8%)	**76.8 ± 7.4**	n/a	n/a
PCC09-06	15	14.35 (2066)	5.021 (723)	0.4710 (3014)	8.4% (23.6%)	**80.6 ± 9.6**	n/a	n/a

Note: The P1 and P2 ages are recalculated central ages where the number of grains in each population were extracted from samples with mixed age distributions using the mixture modeling algorithm of Sambridge and Compston (1994) contained in the Isoplot/Ex program (Ludwig, 2012).

(i). Analyses by external detector method using 0.5 for the $4\pi/2\pi$ geometry correction factor.

(ii). Ages calculated using dosimeter glass: IRMM541 with ζ_{541} = 121.1 ± 3.5 (zircon).

(iii). $P\chi^2$ is the probability of obtaining a χ^2 value for v degrees of freedom where v = no. of crystals – 1.

(iv). n/a = Not applicable as all grains belong to single population.

of Westport, an ~800 m thick section below the detachment is exposed. There, the Buckland Granite contains a cataclastic foliation expressed by aligned and strongly hydrothermally altered potassium feldspar, cataclastically deformed quartz and aligned, shredded chlorite. Aligned, strongly seriticized feldspar and broken ribbon quartz make up a NE-trending stretching lineation on the foliation planes and Riedel-type shear bands provide a top-to-the-NE sense of shear.

Structurally deeper in the footwall at Buckland Peaks, the granite is undeformed to very mildly deformed. In places, white mica is bent, kinked, broken and recrystallized and preferentially aligned. Secondary muscovite and sericite is replacing feldspar. Furthermore, there are isolated patches of dynamically recrystallized quartz and lobate grain boundaries.

Farther south near Mount Kelvin and Mount Raoulia (Fig. 2), the Buckland Granite shows a subhorizontal foliation subparallel to the surrounding CMG rocks and, in general, similarly subtle microscopic deformational features than at Buckland Peaks (Fig. 4E). Despite the proximity of the Ohika Detachment, mesoscopic structures indicate a top-to-the-SW sense of shear for the Buckland Granite. Feldspar porphyroclasts have sigmoidal shapes with asymmetric recrystallized tails and foliation-parallel pegmatite shows C/S-structures (Fig. 4F). The adjacent CMG orthogneiss is significantly more strongly deformed than the Buckland Granite. The gneiss shows a strong, in part mylonitic foliation, which is tightly and complexly folded on a submeter scale with subparallel axial planes striking approximately NE-SW (Fig. 4G). Mesoscopic shear sense indicators include shear bands and asymmetric feldspar porphyroclasts yielding a consistent top-to-the-SW movement. Thin sections reveal biotite-sillimanite aggregates, ribbon quartz, and asymmetric porphyroclasts of dynamically recrystallized feldspar, which also indicate top-to-the-SW sense of shear (Fig. 4H).

Footwall of Pike Detachment

At the southern end of the PCC, deformation proceeded under significantly higher temperatures. Again, deformation is distinctly heterogeneously distributed with a general increase toward the Pike Detachment.

The CMG gneiss near Charleston shows ductile deformation. The preferential orientation of mica grains constitutes a foliation, which is gently folded about NW-SE–trending axes. NE-SW–trending stretching lineations can be observed on the foliation planes. Muscovite flakes are shattered and partly replaced by biotite (Fig. 5A) and bands of recrystallized quartz occur in the domains of more intense deformation. Prominent shear bands and mica fish indicate a consistent top-to-the-SW sense of shear (Fig. 5B). Pegmatite dikes in paragneiss are boudinaged and individual feldspar aggregates are displaced at the decimeter to decameter range, leaving cm- to dm-sized rafts of feldspar floating within the paragneiss. Asymmetries of the boudinaged pegmatite indicate top-to-the-SW shear. However, in places the rocks are barely affected by deformation and display igneous-like textures. Most rocks show weak signs of brittle overprinting and hydrothermal alteration, sericitization and formation of vermicular chlorite (Fig. 5C).

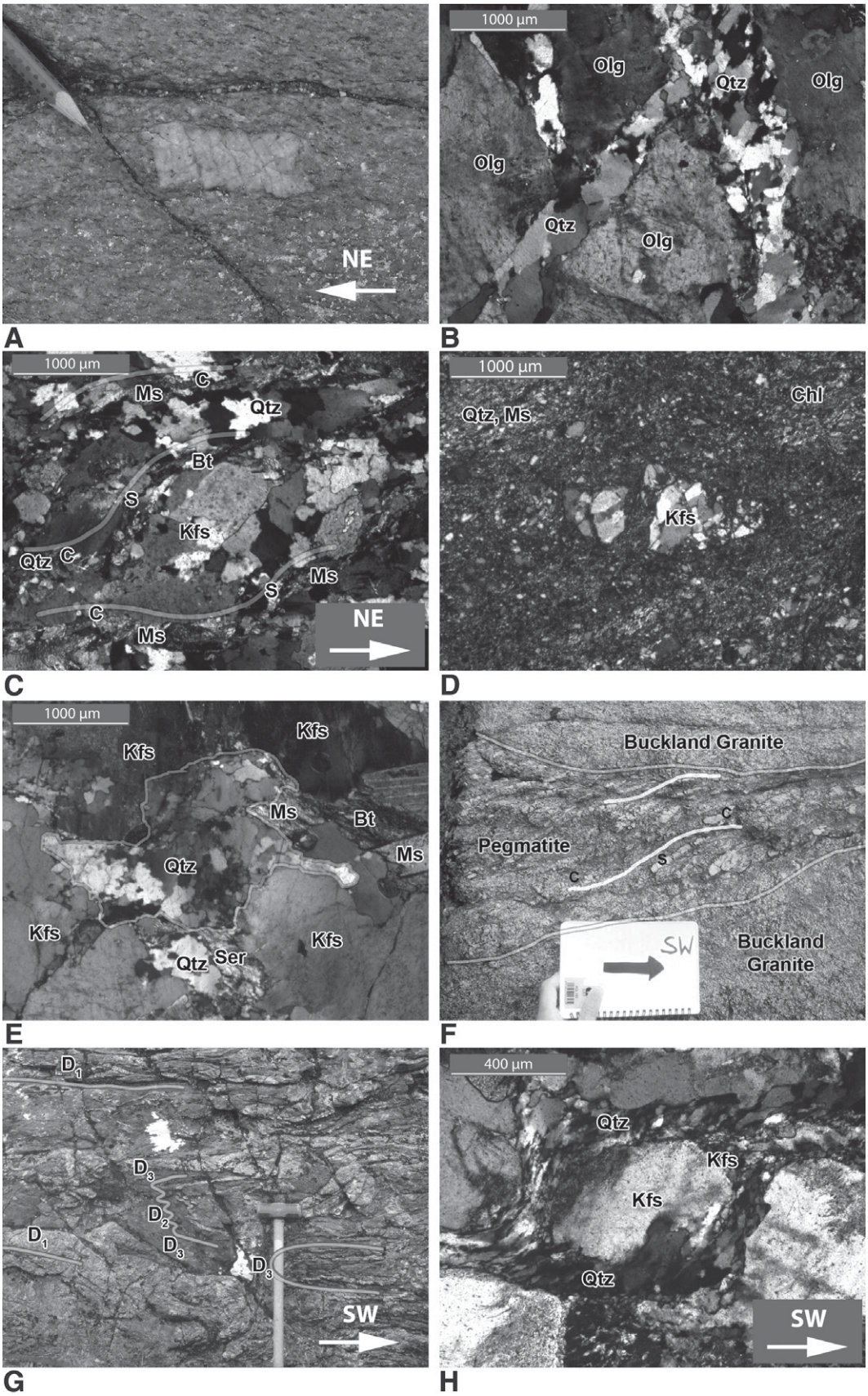

Figure 4. Structures below the Ohika Detachment. (A) Aligned oligoclase porphyroclast with bookshelf structure indicating top-to-the-NE sense of shear. (B) Recrystallized quartz filling brittle fractures of oligoclase. (C) Shear bands indicating top-to-the-NE shear-sense. (D) Ultracataclasite: shattered angular potassium feldspar fragments in a matrix of comminuted quartz, chlorite, and mica constituting a foliation. (E) Isolated patch of dynamically recrystallized quartz with broken and recrystallized muscovite partly replaced by biotite (F) foliation-parallel pegmatite with well-developed C/S-structures indicating top-to-the-SW sense of shear. (G) Charleston Metamorphic Group gneiss tightly folded on a submeter scale, $D_{1–3}$ indicating the sequence of deformation. (H) Porphyroclast of dynamically recrystallized feldspar and quartz indicating top-to-the-SW sense of shear. Bt—biotite; Chl—chlorite; Kfs—K-feldspar; Ms—muscovite; Olg—oligoclase; Qtz—quartz.

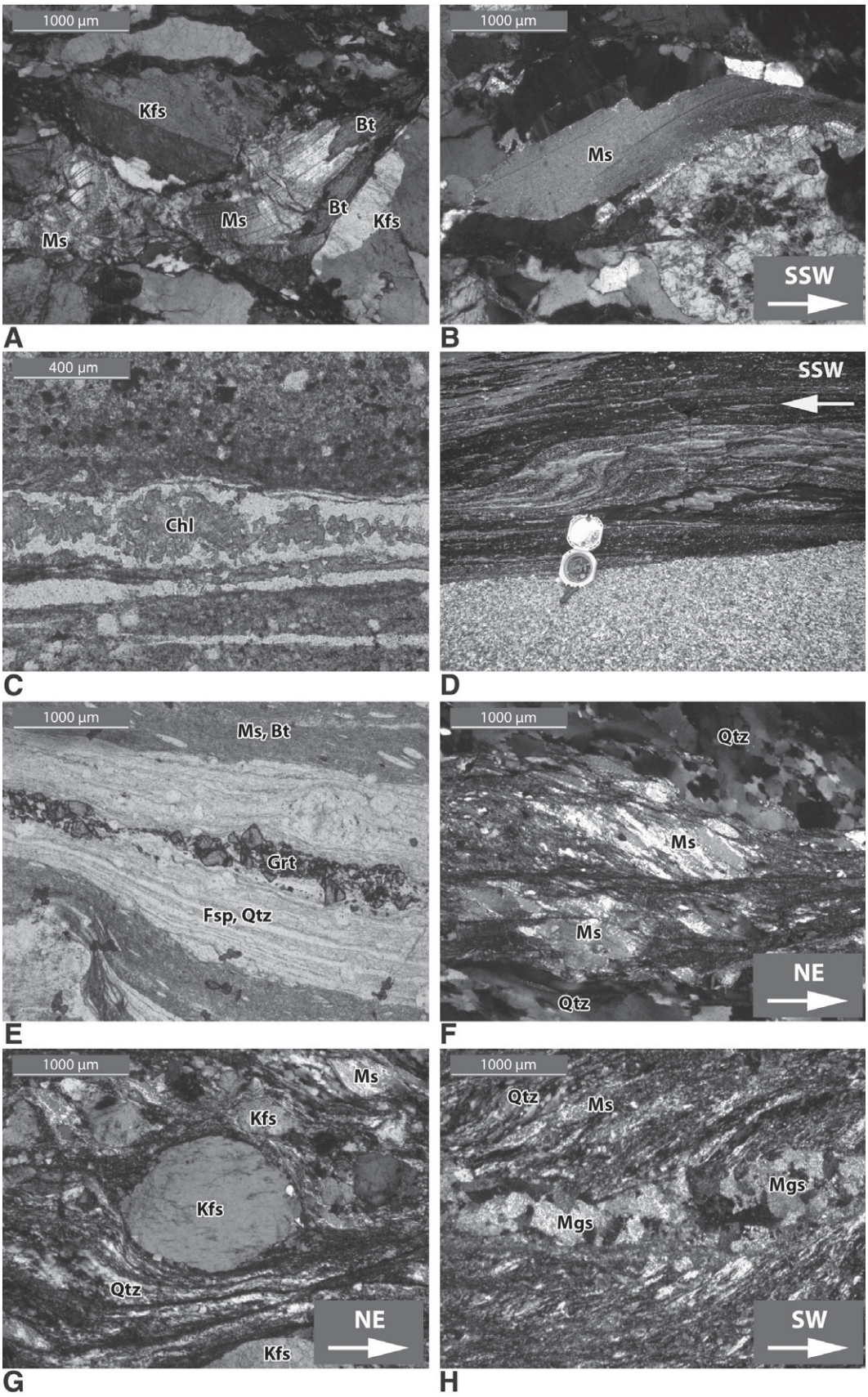

Figure 5. Structures below the Pike Detachment. (A) Shattered muscovite flakes partly replaced by biotite. (B) Mica fish indicating top-to-the-SW sense of shear. (C) Vermicular chlorite. (D) Folding in ultramylonites indicating top-to-the-SSW shear-sense. (E) Extremely fine-grained and pervasively sheared mica- and quartzofeldspathic bands with comminuted and dispersed garnet grain. (F) C/S- structures and oblique foliation indicating top-to-the-SW sense of shear. (G) Feldspar porphyroclast indicating top-to-the-SW sense of shear. (H) C/S-structures and horizontal magnesite vein. Bt—biotite; Chl—chlorite; Grt—garnet; Kfs—K-feldspar; Mgs—magnesite; Ms—muscovite; Qtz—quartz.

The CMG gneiss at Mount Euclid in the Paparoa Range occupies a similar structural level as the coastal section near Charleston. A subhorizontal foliation is defined by aligned biotite, recystallized feldspar and quartz. The foliation is isoclinally folded on a submeter scale. Asymmetric recrystallized potassium feldspar porphyroclasts and C/S-structures defined in part by sillimanite indicate a top-to-the-SW sense of shear.

Ductile deformation and metamorphic conditions become significantly stronger/higher along the coast between Charleston and Fox River Mouth. At Morrisey Creek, the coarse-grained orthogneiss displays a protomylonitic to mylonitic fabric with bands of dynamically recrystallized quartz and undulose extinction and dynamic recrystallization of potassium feldspar. Abundant pegmatite intruded the sequence during progressive deformation. Early pegmatite depicts asymmetric feldspar aggregates and top-to-the-SW shear. Subsequent pegmatite in part intruded along cracks that are inclined 20–30° to the mylonitic foliation (i.e., the pegmatite intruded into shear bands). Ultramylonites (Fig. 5D) formed heterogeneously from granite between White Horse Creek and Morrisey Creek. Here, the host granite grades from mildly deformed to severely deformed granite (orthogneiss) over distances of 0.5–2 m perpendicular to the foliation. With increasing deformation the granitic gneiss grades into black, extremely fine-grained ultramylonite, the latter of which can form 10–25 m thick sheets between the granitic gneiss. The entire rock deformed ductilely and only garnet remained brittle. The garnet is commonly comminuted to angular shards and dispersed along the shear direction. In thin section, the matrix of the ultramylonite is made up of extremely fine-grained and pervasively sheared mica and quartzofeldspathic bands, which constitute a foliation (Fig. 5E). Within the matrix, large white mica fish (typically ~0.5–1 mm) and asymmetric feldspar porphyroclasts (up to 5 cm in diameter) occur and indicate a top-to-the-SW sense of shear. Large plagioclase grains are shattered.

South of White Horse Creek, the intensity of ductile deformation decreases to mylonites and protomylonites. Throughout the entire examined coastal section, stretching lineations trend SW to S and C/S-structures, porphyroclasts, oblique foliations and mica fish yield a consistent top-to-the-SW sense of shear (Figs. 5F, 5G). All rocks show features of hydrothermal alteration such as replacement of biotite by oxides, oxychlorite, and magnesite veins (Fig. 5H).

A distinct brittle overprint becomes increasingly pervasive toward the Pike Detachment. South of White Horse Creek, granitic rocks show pronounced hydrothermal alteration and cataclastic deformation. The ductile foliation is cut by brittle low- and high-angle normal faults. Striations associated with brittle slip indicators on these normal faults are compatible with a top-to-the-SW normal movement. Pegmatite dikes show severe brittle deformation and are boudinaged at a 10–100 m scale. Individual boudins are, in part, asymmetric in shape and this asymmetry is again compatible with a top-to-the-SW sense of shear.

Interpretation and Location of Hinge Zone

Deformation of a wide area in the footwall of the Pike Detachment shows consistent and distinct top-to-the-SW sense of shear indicators that started to develop under upper amphibolite facies conditions. Toward the Pike Detachment the rocks are hydrothermally altered and show a pervasive brittle overprint. Deformation in the footwall of the Ohika Detachment is distinctly weaker than in the footwall of the Pike Detachment. In the direct footwall of the detachment the granite is severely hydrothermally altered and shows pronounced cataclastic deformation as well as brittle and semi-ductile top-to-the-NE shear-sense indicators. At Siberia Bay, top-to-the-NE shear proceeded under lower greenschist facies conditions.

The Buckland Granite is in large parts undeformed. At its northern end the granite shows occasional brittle-ductile top-to-the-NE shear sense indicators. In contrast, at its southern end it shows top-to-the-SW shear-sense indicators and recrystallized potassium feldspar indicates temperatures exceeding 450 °C (Pryer, 1993). Deformation in the southern parts of the Buckland Granite is markedly weaker than in the adjacent orthogneiss, the latter of which shows strong top-to-the-SW shear sense structures that developed under amphibolite-facies conditions.

The reversal of the shear sense indicators defines a hinge zone parallel to the detachments in the northern PCC, which due to the outcrop conditions we can only constrain to a 5-km-wide belt near Buckland Peaks. The strong and distinct top-to-the-SW shear sense indicators in the CMG gneiss in between apophyses of Buckland Granite developed under amphibolite facies conditions and thus at a deep structural level. The considerably weaker deformation fabrics in the granite itself apparently formed at slightly shallower crustal depths. This suggests that the amphibolite facies structures in the CMG gneiss started to form at a deep level, the gneiss continued to be deformed during exhumation and then the Buckland Granite intruded the gneiss during ongoing top-to-the-SW shear.

We did not observe shear-sense indicators that crosscut or overprint each other. However, the top-to-the-NE fabrics in the direct footwall of the Ohika Detachment formed at much shallower crustal depths than the top-to-the-SW structures south of the proposed hinge zone. The same general observation has been made in the Buckland Granite itself, where top-to-the-NE structures in the north developed at brittle-ductile conditions whereas top-to-the-SW shear sense indicators at the southern end of the granite developed at >450 °C as indicated by synkinematically recrystallized potassium feldspar. This pattern suggests northward tilting of the Buckland Granite and also a general northward tilt of the entire PCC.

Rb-Sr DEFORMATION AGE

Sample PCC06-2 is a blackish ultramylonite from south of Morrisey Creek (Fig. 2). The ultramylonite derived from the local Paleozoic granite and has a very fine-grained, dark matrix containing ~5% of coarser components that escaped an otherwise extreme grain-size reduction. The coarser components are asymmetric feldspar porphyroclasts showing a top-to-the-SW shear, some quartz crystals and muscovite fish, the latter appearing as synfolial crystals up to 500 µm in size. Feldspar recrystallized thoroughly indicating deformation well in amphibolite facies conditions.

Rb-Sr isotopic data are presented in Table 3 and Figure 6. The fine-grained matrix, feldspar, and three muscovite grain-size fractions yield an age of 116.2 ± 5.9 Ma (2σ). The three muscovite grain-size fractions essentially define this age

TABLE 3. Rb/Sr ANALYTICAL DATA (ULTRAMYLONITE OF SAMPLE PCC 06-2)

Analysis No.	Material	Rb (ppm)	Sr (ppm)	$^{87}Rb/^{86}Sr$	$^{87}Sr/^{86}Sr$	$^{87}Sr/^{86}Sr$ $2\sigma_m$ (%)
1475	wm 160–80 µm	251	99.0	7.36	0.750800	0.0014
1477	wm 250–160 µm	319	32.2	28.9	0.784673	0.0014
1481	feldspar 250–500 µm	131	317	1.2	0.739992	0.0012
1482	dark matrix (wr) to clasts	241	64.6	10.8	0.755216	0.0014
1483	wm 250–500 µm	350	24.0	42.7	0.809110	0.0016

Note: From sample no. PCC 06-2 (ultramylonite; 116.2 ± 5.9 Ma; MSWD = 27, Sr_i = 0.7379 ± 0.0018). An uncertainty of ± 1.5% (2σ) is assigned to Rb/Sr ratios. Wm—white mica; wr—whole rock.

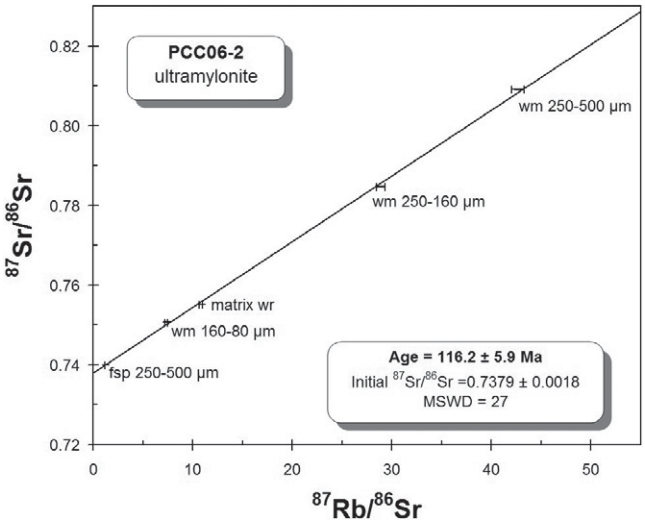

Figure 6. Rb-Sr isochron diagram for ultramylonite PCC06-2 (south of Morrisey Creek, Fig. 2). The ultramylonite evolved from the local Paleozoic granite and shows clasts of white mica (wm) and feldspar in a very fine-grained dark matrix. The elevated MSWD is due to slight Sr-isotopic disequilibria among the analyzed systems, which may reflect the disequilibrium texture of the rock. See text for discussion.

but show largely and systematically different Rb, Sr trace element concentrations and Rb-Sr ratios (Table 3), which is characteristic for progressive synkinematic recrystallization (Glodny et al., 2008b). Sr-isotopic inheritance from pre-Cretaceous events can be ruled out, both for feldspar and muscovite. Although there is some scatter of the data outside analytical uncertainty, possibly reflecting the disequilibrium texture of the rock, we interpret the age of 116.2 ± 5.9 Ma as dating the end of a pre-ultramylonitic, early stage of deformation at amphibolite facies conditions. Ductile shearing therefore initiated prior to the above age and first led to a protomylonitic rock at 116.2 ± 5.9 Ma, which was later on converted to the present ultramylonite during ongoing top-to-the-SW shear.

FISSION-TRACK DATA

Apatite Fission-Track Ages

Apatite fission-track (AFT) ages along the coastline are between 80 and 72 Ma (Table 1) with an average age of ca. 75 Ma. Samples from the lower Buller Gorge area provide Cenozoic ages. These samples fail the χ^2-test, i.e., yield low Pχ^2 values <5% indicating that they have been partially reset by a later heating event. These samples contained only very few older Cretaceous ages and because of the possibility of partial resetting, we did not attempt to deconvolute an older age population from the samples from the Buller Gorge, and they are not further discussed.

Our AFT ages are in general agreement with previous ages in the region (cf. Seward, 1989; Seward and White, 1992). The AFT ages show a weak younging trend from north to south toward the Pike Detachment, which is consistent with the top-to-the-SW shear-sense at the detachment. Even the samples from Cape Foulwind fit the southwestward younging trend, despite the top-to-the-NE shear-sense there. The younging trend extends even beyond the Pike Detachment into the Hawks Craig Breccia at Fox River mouth where sample PCC08-12 yields the second youngest age of 73.0 ± 9.4 Ma. The trend continues farther south as Seward (1989) reported AFT ages from the Meybille Granite as young as 68.8 ± 8.6 Ma (2σ). The Barrytown Granite ~15 km south of the Meybille Granite yields distinctly older AFT ages of 99.5 ± 20.8–93.2 ± 14.2 Ma (2σ). The mean track length data from our samples (Table 1, Fig. 7) are, however, consistent with only moderately fast cooling rates, with mean lengths between 13 and 13.5 µm. This is more typical of cooling rates associated with erosion or cooling by thermal relaxation, rather than the very fast cooling rates that would be expected as a result of tectonic unroofing, where mean track lengths of 14–15 µm would be expected.

Zircon Fission-Track Ages

Zircon fission-track ages (ZFT) are between 125–74 Ma (Table 2, Fig. 8). Several samples fail the χ^2-test indicative of a mixed population of ZFT single grain ages. However, Cretaceous P1 age peaks and their respective errors were extracted from these samples (see Table 2), and are incorporated in the discussion. Except for PCC08-3 the fractions of the grains with mid- to Late Cretaceous ages in the partially reset samples are high (i.e., >0.85) and the errors are comparable to those of the other samples with single population central ages We note that samples PCC06-15 and PCC06-16 were taken inland near the lower Buller Gorge and show slightly younger P1 ages of 75–73 Ma. Seward and White (1992) have previously suspected ZFT ages to be partially annealed in this area during Cenozoic burial. The ZFT ages scatter between 106–76 Ma with a mean at 87 Ma. However, no spatial distribution pattern of the central ages is discernable. Also, sample PCC08-12 from the Hawks Crag Breccia at Fox River mouth (upper plate) shows a ZFT age of 85.7 ± 9.6 Ma, which is the same as the ages of the lower plate. This implies that the upper and lower plates in this area have a common Late Cretaceous thermal history. The individual sample ZFT central ages (including 5 deconvoluted P1 ages) range between 104 and 73 Ma (Fig. 8A). This is also seen in a plot of all the individual grain ages from the same samples (Fig. 8B). The older end of this age range (ca. 103–104 Ma) coincides well with the waning stages of initial unroofing of the basement during the late core complex stage, while the ages at the younger end of the range are coeval within error with the inception of seafloor spreading at ca. 84 Ma (Gaina et al., 1998), and the moderately fast cooling recorded by our AFT ages. We observe no obvious geographic trend or pattern in the ZFT ages. However, the majority of single grain ZFT ages skew toward 70–80 Ma, suggesting most samples must have experienced temperatures close to, or in excess ca. 240 °C during Late Cretaceous reheating.

DISCUSSION

How Symmetric is the Paparoa Core Complex?

Previous work by Tulloch and Kimbrough (1989) and Spell et al. (2000) showed that the PCC is a bivergent, largely symmetric metamorphic core complex. Our new data confirm the bivergent nature of the PCC, but also indicate major differences of the two detachments on either side of the PCC. Top-to-the-SW kinematic indicators related to the Pike Detachment can be traced far into the northern half of the PCC (Fig. 2A), constraining the structural hinge between the two detachment systems to near Buckland Peaks and allocating the southwestern Buckland Granite to the footwall of the Pike Detachment rather than to the Ohika Detachment. This demonstrates that despite the bivergent nature of the PCC an overall asymmetry becomes apparent.

The asymmetry is a result of the dominant control of the Pike Detachment on the extension and the unroofing of the core complex while the northern Ohika Detachment appears to be a late and minor structure (Fig. 9). Nonetheless, previous workers proposed that the Ohika Detachment predates the Pike Detachment (Spell et al.,

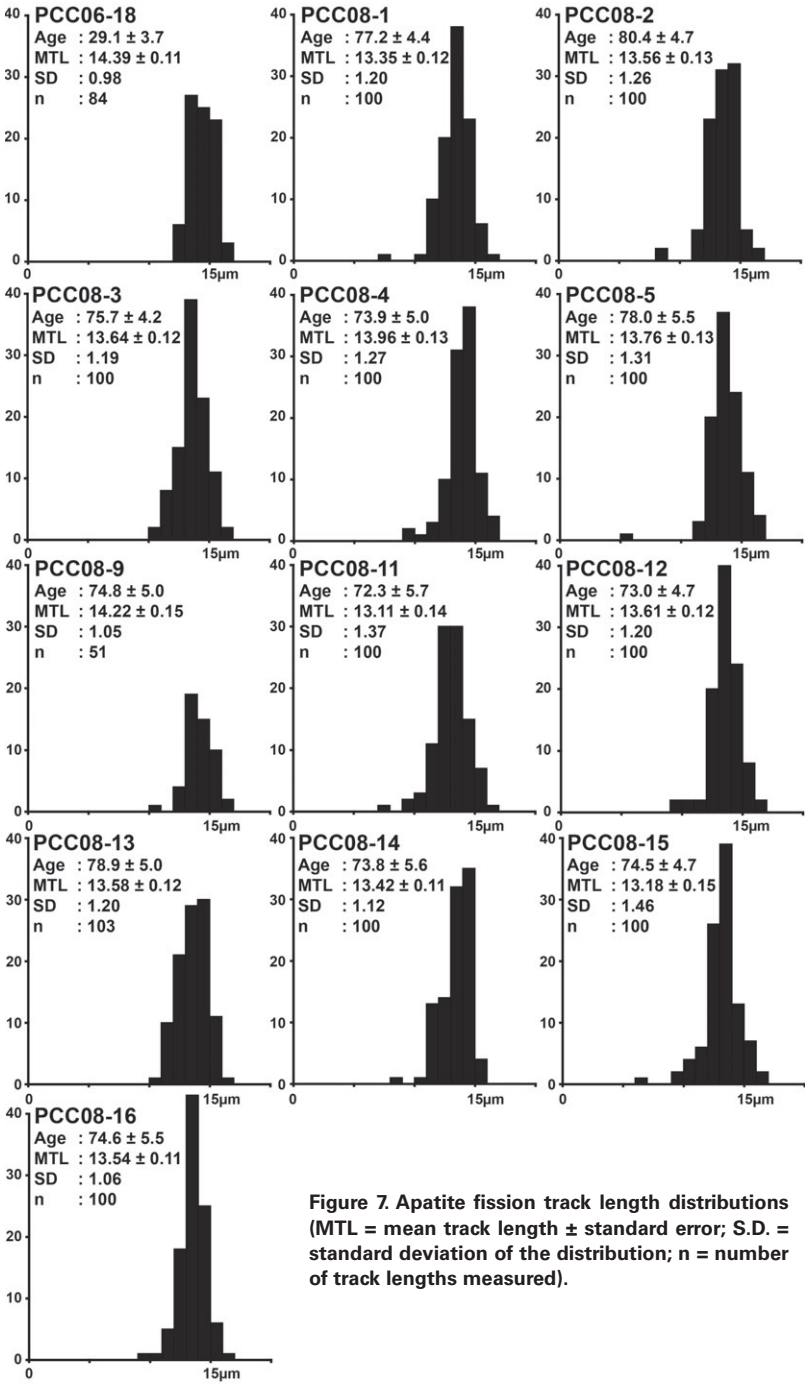

Figure 7. Apatite fission track length distributions (MTL = mean track length ± standard error; S.D. = standard deviation of the distribution; n = number of track lengths measured).

2000; Tulloch and Palmer, 1990). The age of 108.91 ± 0.04 Ma by Buchwaldt et al. (2011) for hydrothermal alteration related to movement of the Ohika Detachment suggests inception of the detachment by ca. 109 Ma. However, an age of 109 Ma is not in line with a Motuan depositional age for the Pororari Group and ages of 102–101 Ma for the Stitts tuff near the base of the Pororari Group. The latter consists of overlapping alluvial and lacustrine fans (Laird, 1995). Fault-bound alluvial fans and deltas are prone to erosion caused by fault parallel basin drainage and environmental changes like water level fluctuations (Gawthorpe and Leeder, 2000). Hence, it is conceivable that the contact of the Stitts Tuff near the base of the Pororari Group probably represents an unconformity. Also earlier splays of the Ohika Detachment may be hidden farther to the north accounting for the gap between the U-Pb zircon ages and the Motuan depositional ages.

Inception of the Pike Detachment and ultramylonitic deformation has been under way by 116.2 ± 5.9 Ma. An age >110 Ma for early movement on the Pike Detachment would largely be in line with Urutawan (as early as 108.4 Ma) ages for the Pororari Group breccias in the hanging wall of the detachment (Raine, 1984). Synmetamorphic mylonitic deformation near Charleston has been dated at 107 ± 2 Ma with a late-tectonic dike cutting the mylonitic foliation at 105 ± 2 Ma (Sagar and Palin, 2011). All these ages collectively suggest that movement on the Pike Detachment was already under way by 116 ± 6 Ma and lasted until ca. 105 Ma. Therefore, based on all available age constraints (Fig. 3), it appears that the Pike Detachment is older than the Ohika Detachment but final movement on both detachments may have overlapped in time.

An age >116 ± 6 Ma for the onset of extensional deformation in the Paparoa Range has implications for the question whether regional extension in New Zealand was syn- or post-subduction. Mortimer et al. (2006), Cawood et al. (1999) and Adams et al. (2009) showed that subduction along the New Zealand sector of the Gondwana margin continued after ca. 110 Ma. Therefore, the onset of extension in the Paparoa Range is concurrent with subduction-related accretion elsewhere and is thus synsubduction. Hence, the early stage of PCC detachment faulting can be considered a result of intra-arc extension as has been proposed for the Basin and Range Province (Zoback et al., 1981).

How does the age of 110 Ma for the Buckland Granite fit into a scenario of two detachments moving at different times? Our structural mapping at the southern end of the Buckland Granite yielded top-to-the-SW kinematic indicators. The adjacent orthogneiss at Mount Kelvin, into which the Buckland Granite intruded, was much more strongly deformed during top-to-the-SW extensional deformation. This strongly suggests that mylonitic top-to-the-SW shearing was already under way before the Buckland Granite intruded at 110 Ma and that the latter intruded into a top-to-the-SW shear zone. A kinematic control of the top-to-the-SW Pike Detachment on the intrusion and deformation of the Buckland Granite would explain the suggested northward dip of the granite. Such a scenario fits with an earlier onset of shearing on the Pike Detachment.

We envisage the following scenario for the Pike Detachment and the intrusions of the Charleston Orthogneiss protolith and the Buckland Granite (Fig. 9). There is a coincidence in time of emplacement of the Charleston Orthogneiss protolith and mylonite deformation of the Pike Detachment footwall at 118 ± 2 Ma (Sagar and Palin, 2011) and 116 ± 6 Ma (our work).

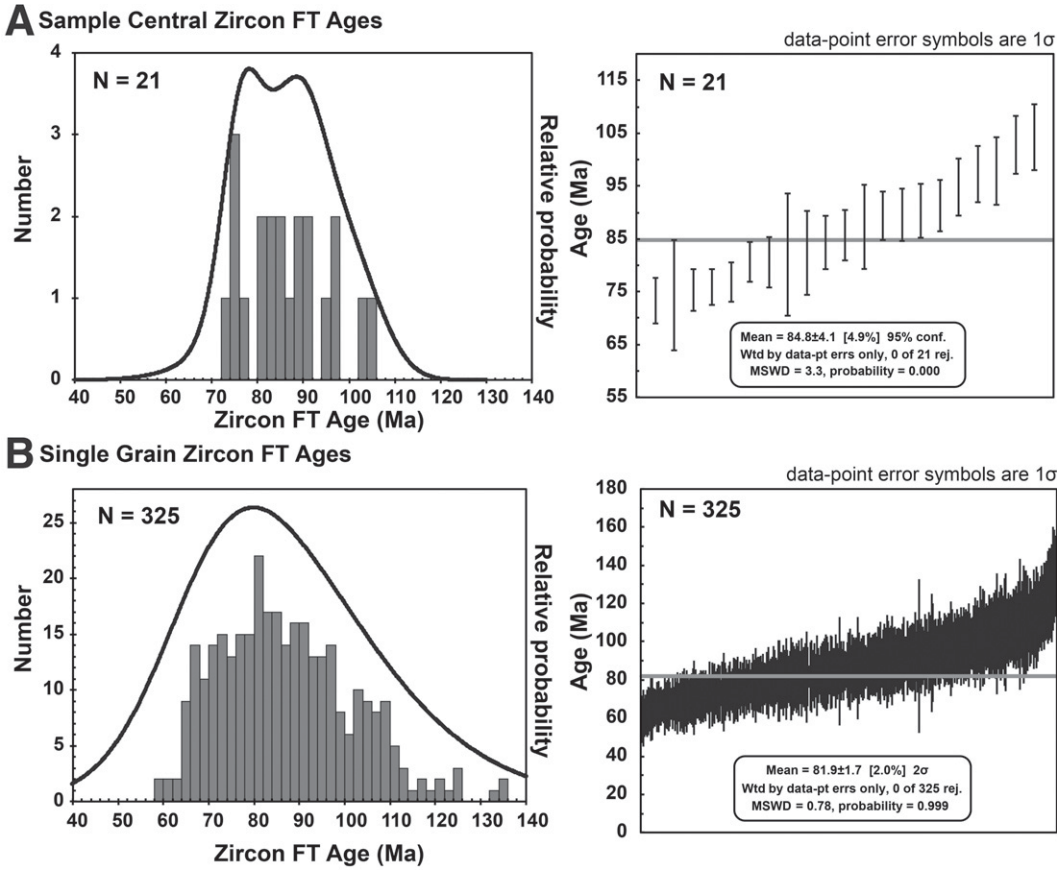

Figure 8. (A) Probability density function and age histogram of sample central zircon fission track (ZFT) ages given in Table 2 including the deconvoluted P1 ages. The plot to the right shows ages with 1σ uncertainty with weighted mean age (calculated using Isoplot/Ex, Ludwig, 2012). (B) Plots showing individual ZFT grain ages from the same samples (N = number of data points/ages)

We argue that this magmatic activity resulted in a transient increase of the geothermal gradient, resulting in migmatization, thermal weakening and the inception of ductile low-angle extensional shearing along the Pike Detachment. Thomson and Ring (2006) described a similar relationship between dike intrusion and low-angle normal shearing in the Aegean extensional province in west Turkey. Parsons and Thompson (1993) proposed that synextensional magmatism, and in particular dike intrusion, can provide the stress heterogeneity required to initiate low-angle normal shearing.

Renewed widespread synkinematic footwall magmatism in the form of the 110 Ma Buckland Granite, perhaps at this time in response to crustal extension, appears ultimately to have led to uplift and doming of the Pike Detachment footwall. Metamorphism of the CMG near Charleston occurred slightly later at 107 ± 2 Ma (Sagar and Palin, 2011) and suggests a link between the intrusion of the Buckland Granite at 110 Ma and high-grade metamorphism. The ages of 107 ± 2 Ma and 105 ± 2 Ma by Sagar and Palin (2011) and the depositional ages of the Pororari Group indicate continued movement at the Pike Detachment until ca. 105 Ma.

The earliest onset of shearing at the Ohika Detachment would be at ca. 109 Ma and thus ~1 m.y. after the intrusion of the Buckland Granite. It appears as if the emplacement of the Buckland Granite in the mid-crust caused uplift and doming and triggered the inception of the Ohika Detachment. Teyssier et al. (2005) argued that extension-induced decompression of deep rocks enhances partial melting and triggers diapiric instabilities to accommodate crustal extension and thinning. The vertical low-viscosity upward flow (doming) would apply a shear stress on the adjacent upper rigid crust and eventually triggers detachment faulting. This would also imply that the hinge zone is typically located close to the synkinematic pluton. Such tectonic scenarios have been demonstrated in other extensional provinces like the Basin-and-Range province and the Aegean Sea region (Brichau et al., 2010; Reynolds and Rehrig, 1980). However, the erosion of the entire upper section of the Buckland intrusion renders our proposition speculative. Given that deposition of the breccias of the Pororari Group above the detachment continued after 102–101 Ma and that the sedimentary rocks are tilted back into the core complex suggests ongoing activity on the Ohika Detachment until ca. 100 Ma.

Pronounced asymmetries in the tectonic evolution of the PCC are also evident from the clasts in the breccias of the Pororari Group (Laird, 1994). Abundant pebbles of Buckland Granite in the hanging wall of the Pike Detachment indicate that large parts of the breccia were deposited after 110 Ma in graben above the Pike Detachment.

Our model acknowledges the bivergent overall architecture of the PCC as proposed by Tulloch and Kimbrough (1989) and Spell et al. (2000). However, our model highlights distinct asymmetries and places a dominant role on the Pike Detachment.

Differential Exhumation

The level of footwall exhumation beneath the two PCC detachments is also different, supporting our model of pronounced asymmetry of the bivergent PCC. Top-to-the-NE kinematic indicators in the Cape Foulwind Granite beneath the Ohika Detachment show brittle behavior of feldspar, syndeformational chlorite stability and largely cataclastic deformation structures along the Ohika Detachment in the Buckland Granite. Overall, this suggests lower greenschist facies conditions (~350 °C). Based on thermobarom-

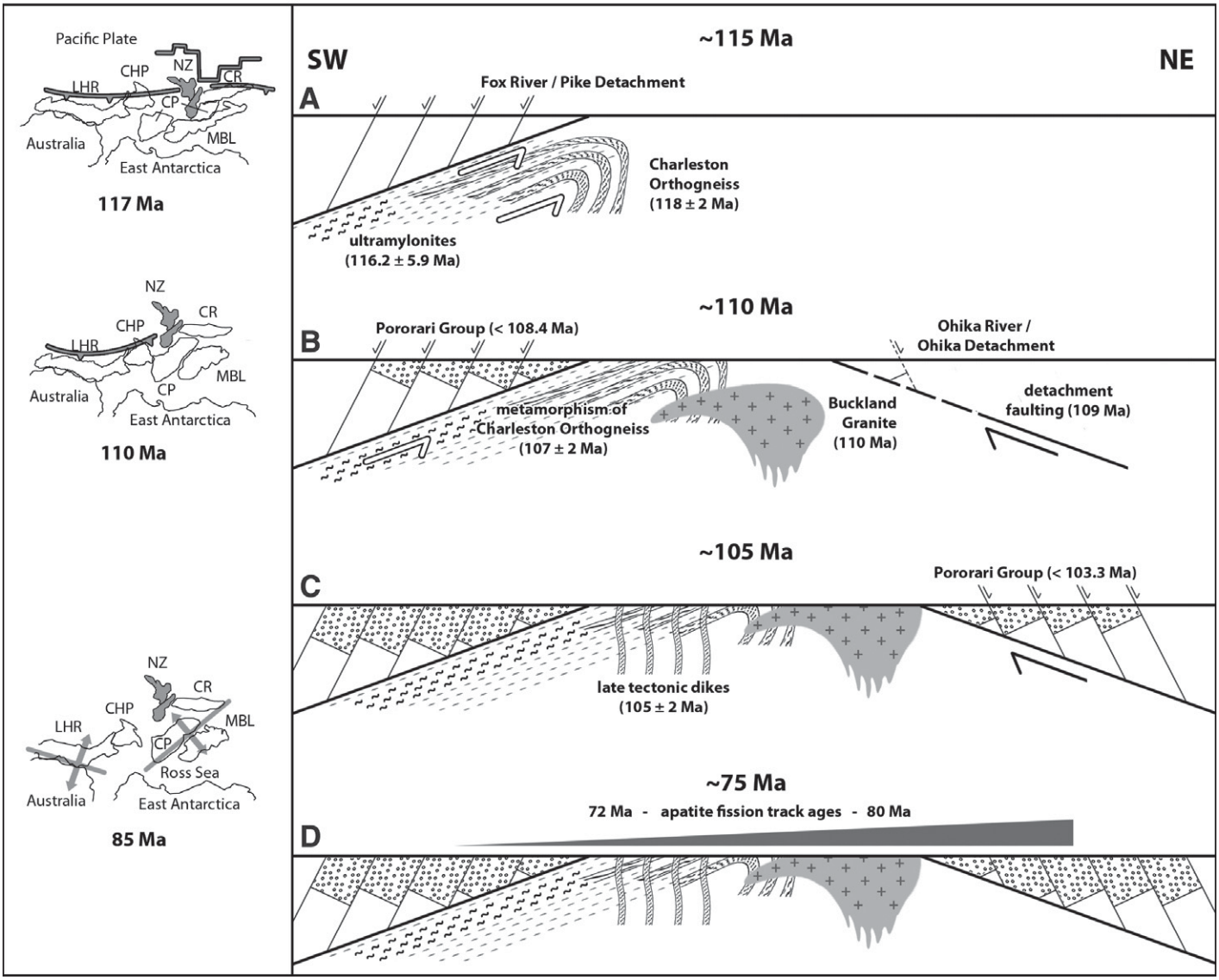

Figure 9. Schematic (not scaled) sequence of the core complex development and corresponding paleogeography (after Gaina et al., 1998; Mukasa and Dalziel, 2000). (A) Normal faulting on the Pike Detachment, formation of ultramylonite and intrusion of orthogneiss protolith. (B) Emplacement of the Buckland Granite during top-to-the-SE shear and metamorphism of the Charleston Orthogneiss at 110 Ma and 107 ± 2 Ma; inception of the Ohika Detachment at 109 Ma. (C) Final stages of activity at Ohika Detachment. (D) Resetting of fission-track ages during Late Cretaceous thermal pulse probably associated with initial seafloor spreading in Tasman Sea and associated magmatic activity in South Island. CHP—Challenger Plateau; CR—Chatham Rise; CP—Campbell Plateau; LHR—Lord Howe Rise; MBL—Mary Byrd Land; NZ—New Zealand.

etry of the CMG, White (1994) estimated a paleothermal gradient of ≥50 °C km^{-1} suggesting an exhumation depth beneath the Ohika Detachment of ~7 km. Assuming a syndeformation dip of 30° for the Ohika Detachment suggests a maximum displacement of 14 km.

In contrast, the formation of ultramylonites at Morrisey Creek was associated with the development of feldspar porphyroclasts and the complete recrystallization of former magmatic feldspar. This together with the migmatites and the sillimanite isograd (White, 1994) suggests temperatures in excess of 650 °C in the footwall of the Pike Detachment. Applying a paleothermal gradient of 50 °C km^{-1} results in >~13 km of footwall exhumation. Assuming again a syndeformation dip of 30° for the Pike Detachment suggests a minimum displacement of 26 km.

We note that our displacement estimates are crude. They would, however, result in an overall horizontal extension of the PCC of ~40 km, which roughly equals the present length of the PCC, and also places the structural hinge closer to the Ohika Detachment.

We envisage that both detachments were active for ~10 m.y. If the cooling rates of ~100 °C Ma^{-1}and slip rates of > 4 km Ma^{-1} proposed by Spell et al. (2000) are applied, movement on both detachments could not have been continuous over these 10 m.y. as this would result in too much cooling, too much exhumation and too much extension than the current exhumation level and distance between the two detachments would support.

Late Cretaceous Reactivation

AFT ages of 80–72 Ma and the youngest ZFT ages of 74–73 Ma are ~25 m.y. younger

than the main activity of the PCC between ca. 115 and 100 Ma. The latter time span is in accord with usual lifetimes of core complexes worldwide, which are around 5–15 m.y. (Foster and John, 1999; Ring and Bernet, 2010).

Sample PCC08-12 from a clast of Buckland Granite in the Pororari Group also yielded a late Cretaceous ZFT age of 86 Ma and an AFT age of 73 Ma. The clast must have been cooled after ca. 110 Ma and deposited in the Pororari Group before ca. 100 Ma. Its ZFT and AFT ages must have then been reset in the late Cretaceous following deposition together with the other ZFT and AFT ages from the PCC.

Full resetting of the ZFT ages through burial would require an overburden of more than 5 km if a high post-core-complex paleothermal gradient of 50 °C km^{-1} was assumed. For the East Coast of Australia, the geothermal gradient during initial seafloor spreading is estimated to be up to 50 °C km^{-1} (Moore et al., 1986). However, there is no evidence from the entire South Island of New Zealand for such sediment accumulations between ~100–85 Ma. Therefore, it appears more realistic to invoke a reheating event associated with initial spreading in the Tasman Sea and associated lamprophyre dike intrusion along the West Coast of New Zealand. Similar AFT ages of 80–72 Ma occur in several other places on the South Island (Batt et al., 2004; Kamp, 1997), which are unaffected by resetting related to young deformation along the Alpine Fault. Tulloch et al. (2009) reported on a Zealandia-wide spatial distribution of late Cretaceous ages. This promotes the idea of a regional thermal event that reset the AFT ages, and partially-to-fully reset the ZFT ages. Small-scale convection processes in the transition zone between oceanic and continental crust causing persistent thermal anomalies after continental breakup are suspected to be a common feature of continental margins, which can also lead to post-rift magmatism (King and Ritsema, 2000; Lucazeau et al., 2008).

The envisaged Late Cretaceous reheating event did not affect the Ar/Ar and K/Ar muscovite ages from the PCC and the granite clasts in the Pororari Group reported by Tulloch and Palmer (1990) and Spell et al. (2000). This is no surprise since Di Vincenzo et al. (2001) showed that it needs at least 500 °C for diffusional resetting of Ar-Ar ages in muscovite. Instead, deformation-related fluid flow, deformation and recrystallization are critical to reset Ar-Ar ages (Villa, 2010)

The K/Ar sericite ages of 84.9 ± 1.3 Ma and 86.0 ± 1.0 Ma from reworked basement breccias below the Pike Detachment suggests deformation-related hydrothermal activity (Tulloch and Palmer, 1990). The 86–80 Ma old NW-striking lamprophyre dikes suggest a NE-SW extension direction. The spatial distribution of AFT ages between 80 and 72 Ma shows a weak pattern, which is too young to be related to core complex faulting. Likewise, the track lengths support moderate cooling rates rather than rapid ones typical for core complex faulting. Instead, the age pattern and the moderate cooling rates may reflect a higher thermal gradient toward the developing late Cretaceous graben formation or Neogene tilting during the Alpine Fault related Paparoa pop-up structure.

The AFT ages of 80–72 Ma immediately post-date initial rifting in the Tasman Sea at 84 Ma (Gaina et al., 1998) and are therefore likely to be causally related to sea-floor spreading. The tectonic evolution of West Antarctica on the other side of the Tasman Sea rift is remarkably similar and suggests a broad regional event: Crustal extension of hot lithosphere in the mid Cretaceous followed by initial seafloor spreading with regional uplift and cooling recorded by AFT ages of 83–70 Ma (Siddoway, 2008).

The deformation event at ca. 85–70 Ma most probably caused the formation of the Paparoa coal basin south of the Paparoa Range. We propose that at this time parts of the PCC were re-exhumed and caused an increase in the content of metamorphic detritus in the upper parts of the basin fill (Bassett et al., 2006).

CONCLUSIONS

We have shown that the formation of the Paparoa Metamorphic Core Complex was caused by top-to-the-SW displacement along the Pike Detachment starting before 116 ± 6 Ma. Inception of the Pike Detachment possibly coincided with the intrusion of at least parts of the protolith of the Charleston Orthogneiss at 118 ± 2 Ma. We propose that the magmatic activity resulted in a transient increase in the geothermal gradient, resulting in migmatization, thermal weakening and the inception of ductile low-angle extensional shearing along the Pike Detachment. Subsequently, the Buckland Granite intruded in response to the crustal extension at ca. 110 Ma. Emplacement of the Buckland Granite into the mid-crust is suggested to have caused uplift and doming and may have caused the inception of the Ohika Detachment at the northern end of the PCC. The cessation of extension and core complex deformation is poorly constrained but seems to have occurred by ca. 105 Ma at the Pike Detachment and ca. 100 Ma at the Ohika Detachment.

Most of the exhumation of the PCC has been accommodated by top-to-the-SW displacement at the Pike Detachment and caused the exposure of synextensional migmatites in its footwall. Below the Ohika Detachment lower/mid-greenschist facies rocks were exhumed. Differential exhumation resulted in an asymmetric structure of the bivergent PCC. The structural hinge is located relatively close to the northern Ohika Detachment.

The fission-track ages suggest renewed tectonic and thermal activity at the southern end of the PCC during initial seafloor spreading in the Tasman Sea by ca. 84 Ma after a tectonic pause of ~25 m.y. Resetting of the fission-track ages was probably caused by thermal activity associated with elevated heat flow during initial seafloor spreading and lamprophyre dike intrusion.

Overall, the former subduction-related magmatic arc along the West Coast of New Zealand represented an extensional province in the mid- and Late Cretaceous. This extensional province developed during the waning stage of subduction along the Eastern Gondwana margin and is characterized by the widespread development of thinned crust, the formation of core complexes, and associated magmatic activity. Extensional deformation was facilitated by a hot and thermally weak lithosphere.

ACKNOWLEDGMENTS

Fieldwork for this study was supported by the Mason Trust Fund. We want to thank R. Spiers and D. Shelley for the processing and the evaluation of the thin sections and F. Leyrat for assistance in the field. Also thanks to I. Raine for helpful comments on the Late Cretaceous palynology. Jim Vogl and Rory McFadden provided constructive reviews, which are gratefully acknowledged.

REFERENCES CITED

Adams, C.J., Mortimer, N., Campbell, H.J., and Griffin, W.L., 2009, Age and isotopic characterisation of metasedimentary rocks from the Torlesse Supergroup and Waipapa Group in the central North Island, New Zealand: New Zealand Journal of Geology and Geophysics, v. 52, no. 2, p. 149–170, doi:10.1080/00288300909509883.

Adams, C.J.D., and Nathan, S., 1978, Cretaceous chronology of the Lower Buller Valley, South Island New Zealand: New Zealand Journal of Geology and Geophysics, v. 21, p. 455–462, doi:10.1080/00288306.1978.10424070.

Allmendinger, R.W., Cardozo, N.C., and Fisher, D., 2013, Structural Geology Algorithms: Vectors & Tensors, Cambridge, England, Cambridge University Press, 289 p.

Bassett, K., Ettmuller, F., and Bernet, M., 2006, Provenance analysis of the Paparoa and Brunner Coal Measures using integrated SEM-cathodoluminescence and optical microscopy: New Zealand Journal of Geology and Geophysics, v. 49, no. 2, p. 241–254, doi:10.1080/00288306.2006.9515163.

Batt, G.E., Baldwin, S.L., Cottam, M.A., Fitzgerald, P.G., Brandon, M.T., and Spell, T.L., 2004, Cenozoic plate boundary evolution in the South Island of New Zealand: New thermochronological constraints: Tectonics, v. 23, no. 4, TC4001, doi:10.1029/2003TC001527.

Bernet, M., 2009, A field-based estimate of the zircon fission-track closure temperature: Chemical Geology, v. 259, no. 3–4, p. 181–189, doi:10.1016/j.chemgeo.2008.10.043.

Block, L., and Royden, L.H., 1990, Core complex geometries and regional scale flow in the lower crust: Tectonics, v. 9, no. 4, p. 557–567, doi:10.1029/TC009i004p00557.

Bradshaw, J.D., 1989, Cretaceous geotectonic patterns in the New Zealand Region: Tectonics, v. 8, no. 4, p. 803–820, doi:10.1029/TC008i004p00803.

Bradshaw, J.D., 1993, A review of the Median Tectonic Zone: Terrane boundaries and terrane amalgamation near the Median Tectonic Line: New Zealand Journal of Geology

and Geophysics, v. 36, no. 1, p. 117–125, doi:10.1080/00288306.1993.9514559.

Brandon, M.T., Roden-Tice, M.K., and Garver, J.I., 1998, Late Cenozoic exhumation of the Cascadia accretionary wedge in the Olympic Mountains, northwest Washington State: Geological Society of America Bulletin, v. 110, no. 8, p. 985–1009, doi:10.1130/0016-7606(1998)110<0985:LCEOTC>2.3.CO;2.

Brichau, S., Thomson, S., and Ring, U., 2010, Thermochronometric constraints on the tectonic evolution of the Serifos detachment, Aegean Sea, Greece: International Journal of Earth Sciences, v. 99, no. 2, p. 379–393, doi:10.1007/s00531-008-0386-0.

Buchwaldt, R., Ring, U., and Tulloch, A.J., 2011, Decoding the timing within the Paparoa Metamorphic Core Complex, New Zealand: new insights of the break-up of southern Gondwana: Geological Society of America Abstracts with Programs, v. 43, no. 5, p. 653.

Buck, W.R., 1991, Modes of Continental Lithospheric Extension: Journal of Geophysical Research, v. 96, no. B12, p. 20161–20178, doi:10.1029/91JB01485.

Cardozo, N., and Allmendinger, R.W., 2013, Spherical projections with OSXStereonet: Computers & Geosciences, v. 51, no. 0, p. 193–205, doi:10.1016/j.cageo.2012.07.021.

Cawood, P.A., Nemchin, A.A., Leverenz, A., Saeed, A., and Balance, P.F., 1999, U/Pb dating of detrital zircons: Implications for the provenance record of Gondwana margin terranes: Geological Society of America Bulletin, v. 111, no. 8, p. 1107–1119, doi:10.1130/0016-7606(1999)111<1107:UPDODZ>2.3.CO;2.

Cliff, R.A., and Meffan-Main, S., 2003, Evidence from Rb-Sr microsampling geochronology for the timing of Alpine deformation in the Sonnblick Dome, SE Tauern Window, Austria, *in* Vance, D., and Villa, I.M., eds., Geochronology: Linking the Isotopic Record with Petrology and Textures: Geological Society of London, Special Publication 220, no. 1, p. 159–172, doi:10.1144/GSL.SP.2003.220.01.09.

Coney, P.J., 1980, Cordilleran metamorphic core complexes: An overview, *in* Crittenden, M.D., Coney, P.J., and Davis, G.H., eds., Cordilleran Metamorphic Core Complexes: Geological Society of America Memoirs 153, p. 7–31.

Cooper, R.A., 2004, The New Zealand Geological Timescale, Lower Hutt: Institute of Geological & Nuclear Sciences Limited, Institute of Geological & Nuclear Sciences Monograph 22, 284 p.

Di Vincenzo, G., Ghiribelli, B., Giorgetti, G., and Palmeri, R., 2001, Evidence of a close link between petrology and isotope records: constraints from SEM, EMP, TEM and in situ ^{40}Ar-^{39}Ar laser analyses on multiple generations of white micas (Lanterman Range, Antarctica): Earth and Planetary Science Letters, v. 192, no. 3, p. 389–405, doi:10.1016/S0012-821X(01)00454-X.

Fleischer, R.L., Price, P.B., and Walker, R.M., 1975, Nuclear Tracks in Solids: Principles and Applications: Berkeley, University of California Press, 627 p.

Foster, D.A., and John, B.E., 1999, Quantifying tectonic exhumation in an extensional orogen with thermochronology: examples from the southern Basin and Range Province, *in* Ring, U., et al. eds., Exhumation Processes: Normal Faulting, Ductile Flow and Erosion: Geological Society of London, Special Publication 154, no. 1, p. 343–364, doi:10.1144/GSL.SP.1999.154.01.16.

Gaina, C., Müller, D.R., Royer, J.-Y., Stock, J., Hardebeck, J., and Symonds, P., 1998, The tectonic history of the Tasman Sea: A puzzle with 13 pieces: Journal of Geophysical Research–Solid Earth, v. 103, no. B6, p. 12413–12433, doi:10.1029/98JB00386.

Galbraith, R.F., and Laslett, G.M., 1993, Statistical models for mixed fission track ages: Nuclear Tracks and Radiation Measurements, v. 21, no. 4, p. 459–470, doi:10.1016/1359-0189(93)90185-C.

Gawthorpe, R.L., and Leeder, M.R., 2000, Tectono-sedimentary evolution of active extensional basins: Basin Research, v. 12, no. 3–4, p. 195–218, doi:10.1046/j.1365-2117.2000.00121.x.

Gessner, K., Wijns, C., and Moresi, L., 2007, Significance of strain localization in the lower crust for structural evolution and thermal history of metamorphic core complexes: Tectonics, v. 26, no. 2, TC2012, doi:10.1029/2004TC001768.

Ghisetti, F.C., and Sibson, R.H., 2006, Accommodation of compressional inversion in north-western South Island (New Zealand): Old faults versus new?: Journal of Structural Geology, v. 28, no. 11, p. 1994–2010, doi:10.1016/j.jsg.2006.06.010.

Gibson, G.M., McDougall, I., and Ireland, T.R., 1988, Age constraints on metamorphism and the development of a metamorphic core complex in Fiordland, southern New Zealand: Geology, v. 16, no. 5, p. 405–408, doi:10.1130/0091-7613(1988)016<0405:ACOMAT>2.3.CO;2.

Glodny, J., Kühn, A., and Austrheim, H., 2008a, Geochronology of fluid-induced eclogite and amphibolite facies metamorphic reactions in a subduction-collision system, Bergen Arcs, Norway: Contributions to Mineralogy and Petrology, v. 156, no. 1, p. 27–48, doi:10.1007/s00410-007-0272-y.

Glodny, J., Ring, U., and Kühn, A., 2008b, Coeval high-pressure metamorphism, thrusting, strike-slip, and extensional shearing in the Tauern Window, Eastern Alps: Tectonics, v. 27, no. 4, TC4004, doi:10.1029/2007TC002193.

Green, P.F., Duddy, I.R., Laslett, G.M., Hegarty, K.A., Gleadow, A.J.W., and Lovering, J.F., 1989, Thermal annealing of fission tracks in apatite 4. Quantitative modelling techniques and extension to geological timescales: Chemical Geology, Isotope Geoscience Section, v. 79, no. 2, p. 155–182, doi:10.1016/0168-9622(89)90018-3.

Hollis, C.J., Beu, A.G., Crampton, J.S., Jones, C.M., Crundwell, M.P., Morgans, H.E.G., Raine, J.I., and Boyes, A.F., 2010, Calibration of the New Zealand Cretaceous-Cenozoic Timescale to GTS2004.

Hurford, A.J., and Green, P.F., 1983, The zeta age calibration of fission-track dating: Isotope Geoscience, v. 1, p. 285–317.

Ireland, T.R., and Gibson, G.M., 1998, SHRIMP monazite and zircon geochronology of high-grade metamorphism in New Zealand: Journal of Metamorphic Geology, v. 16, no. 2, p. 149–167, doi:10.1111/j.1525-1314.1998.00112.x.

Kamp, P.J.J., 1997, Paleogeothermal gradient and deformation style, Pacific front of the Southern Alps Orogen: Constraints from fission track thermochronology: Tectonophysics, v. 271, no. 1–2, p. 37–58, doi:10.1016/S0040-1951(96)00246-6.

Kamp, P.J.J., Whitehouse, I.W.S., and Newman, J., 1999, Constraints on the thermal and tectonic evolution of Greymouth coalfield: New Zealand Journal of Geology and Geophysics, v. 42, no. 3, p. 447–467, doi:10.1080/00288306.1999.9514855.

Ketcham, R.A., Donelick, R.A., and Carlson, W.D., 1999, Variability of apatite fission-track annealing kinetics; III, Extrapolation to geological time scales: The American Mineralogist, v. 84, no. 9, p. 1235–1255.

King, S.D., and Ritsema, J., 2000, African Hot Spot Volcanism: Small-Scale Convection in the Upper Mantle beneath Cratons: Science, v. 290, no. 5494, p. 1137–1140, doi:10.1126/science.290.5494.1137.

Kingma, J.T., 1959, The tectonic history of New Zealand: New Zealand Journal of Geology and Geophysics, v. 2, no. 1, p. 1–55, doi:10.1080/00288306.1959.10431311.

Kula, J., Tulloch, A., Spell, T.L., and Wells, M.L., 2007, Two-stage rifting of Zealandia-Australia-Antarctica: Evidence from $^{40}Ar/^{39}Ar$ thermochronometry of the Sisters shear zone, Stewart Island, New Zealand: Geology, v. 35, no. 5, p. 411–414, doi:10.1130/G23432A.1.

Laird, M.G., 1968, The Paparoa Tectonic Zone: New Zealand Journal of Geology and Geophysics, v. 11, p. 435–454, doi:10.1080/00288306.1968.10423661.

Laird, M.G., 1994, Geologic aspects of the opening of the Tasman Sea, *in* Van Der Lingen, G.J., Swanson, K.M., and Muir, R.J., eds., Evolution of the Tasman Sea Basin: proceedings of the Tasman Sea Conference, Christchurch, New Zealand, 27–30 November 1992: Rotterdam, Brookfield, A.A. Balkema.

Laird, M.G., 1995, Coarse-grained lacustrine fan-delta deposits (Pororari Group) of the northwestern South Island, New Zealand: evidence for Mid-Cretaceous rifting, *in* Plint, A.G., ed., Sedimentary Facies Analysis: International Association of Sedimentologists Special Publication 22, p. 197–217.

Laird, M.G., and Bradshaw, J.D., 2004, The Break-up of a Long-term Relationship: the Cretaceous Separation of New Zealand from Gondwana: Gondwana Research, v. 7, no. 1, p. 273–286, doi:10.1016/S1342-937X(05)70325-7.

Lavier, L.L., Roger Buck, W., and Poliakov, A.N.B., 1999, Self-consistent rolling-hinge model for the evolution of large-offset low-angle normal faults: Geology, v. 27, no. 12, p. 1127–1130, doi:10.1130/0091-7613(1999)027<1127:SCRHMF>2.3.CO;2.

Lister, G.S., and Davis, G.A., 1989, The origin of metamorphic core complexes and detachment faults formed during Tertiary continental extension in the northern Colorado River region, U.S.: Journal of Structural Geology, v. 11, no. 1–2, p. 65–94, doi:10.1016/0191-8141(89)90036-9.

Lucazeau, F., Leroy, S., Bonneville, A., Goutorbe, B., Rolandone, F., d'Acremont, E., Watremez, L., Düsünur, D., Tuchais, P., Huchon, P., Bellahsen, N., and Al-Toubi, K., 2008, Persistent thermal activity at the Eastern Gulf of Aden after continental break-up: Nature Geoscience, v. 1, no. 12, p. 854–858, doi:10.1038/ngeo359.

Ludwig, K.R., 2012, Isoplot, Special Publication No. 5: Berkeley Geochronology Center, p. A Geochronological Toolkit for Microsoft Excel.

Moore, M.E., Gleadow, A.J.W., and Lovering, J.F., 1986, Thermal evolution of rifted continental margins: new evidence from fission tracks in basement apatites from southeastern Australia: Earth and Planetary Science Letters, v. 78, no. 2-3, p. 255–270, doi:10.1016/0012-821X(86)90066-X.

Mortimer, N., Tulloch, A.J., Spark, R.N., Walker, N.W., Ladley, E., Allibone, A., and Kimbrough, D.L., 1999, Overview of the Median Batholith, New Zealand: a new interpretation of the geology of the Median Tectonic Zone and adjacent rocks: Journal of African Earth Sciences, v. 29, no. 1, p. 257–268, doi:10.1016/S0899-5362(99)00095-0.

Mortimer, N., Davey, F.J., Melhuish, A., Yu, J., and Godfrey, N.J., 2002, Geological interpretation of a deep seismic reflection profile across the Eastern Province and Median Batholith, New Zealand: Crustal architecture of an extended Phanerozoic convergent orogen: New Zealand Journal of Geology and Geophysics, v. 45, no. 3, p. 349–363, doi:10.1080/00288306.2002.9514978.

Mortimer, N., Hoernle, K., Hauff, F., Palin, J.M., Dunlap, W.J., Werner, R., and Faure, K., 2006, New constraints on the age and evolution of the Wishbone Ridge, southwest Pacific Cretaceous microplates, and Zealandia–West Antarctica breakup: Geology, v. 34, no. 3, p. 185–188, doi:10.1130/G22168.1.

Muir, R.J., Ireland, T.R., Weaver, S.D., and Bradshaw, J.D., 1994, Ion microprobe U-Pb zircon geochronology of granitic magmatism in the Western Province of the South Island, New Zealand: Chemical Geology, v. 113, no. 1-2, p. 171–189, doi:10.1016/0009-2541(94)90011-6.

Muir, R.J., Ireland, T.R., Weaver, S.D., Bradshaw, J.D., Waight, T.E., Jongens, R., and Eby, G.N., 1997, SHRIMP U-Pb geochronology of Cretaceous magmatism in northwest Nelson-Westland, South Island, New Zealand: New Zealand Journal of Geology and Geophysics, v. 40, p. 453–463, doi:10.1080/00288306.1997.9514775.

Mukasa, S.B., and Dalziel, I.W.D., 2000, Marie Byrd Land, West Antarctica: Evolution of Gondwana's Pacific margin constrained by zircon U-Pb geochronology and feldspar common-Pb isotopic compositions: Geological Society of America Bulletin, v. 112, no. 4, p. 611–627, doi:10.1130/0016-7606(2000)112<611:MBLWAE>2.0.CO;2.

Müller, W., Dallmeyer, R.D., Neubauer, F., and Thöni, M., 1999, Deformation-induced resetting of Rb/Sr and $^{40}Ar/^{39}Ar$ mineral systems in a low-grade, polymetamorphic terrane (Eastern Alps, Austria): Journal of the Geological Society, v. 156, no. 2, p. 261–278, doi:10.1144/gsjgs.156.2.0261.

Müller, W., Mancktelow, N.S., and Meier, M., 2000, Rb-Sr microchrons of synkinematic mica in mylonites: an example from the DAV fault of the Eastern Alps: Earth and Planetary Science Letters, v. 180, no. 3-4, p. 385–397, doi:10.1016/S0012-821X(00)00167-9.

Naeser, C.W., and Faul, H., 1969, Fission-track annealing in apatite and sphene: Journal of Geophysical Research, v. 74, no. 2, p. 705–710, doi:10.1029/JB074i002p00705.

Nathan, S., 1978, Geological Map of New Zealand, Buller-Lyell, sheets S31 and S32, scale 1:63,360: New Zealand Department of Scientific and Industrial Research, scale 1:63,360.

Nathan, S., Anderson, H.J., Cook, R.A., Herzer, R.H., Hoskins, R.H., and Raine, J.I., 1986, Cretaceous and Cenozoic sedimentary basins of the West Coast region, South Island, New Zealand: New Zealand Geological Survey, Basin Studies no. 1, 90 p.

Parsons, T., and Thompson, G.A., 1993, Does magmatism influence low-angle normal faulting?: Geology, v. 21, p. 247–250, doi:10.1130/0091-7613(1993)021<0247:DMILAN>2.3.CO;2.

Pryer, L.L., 1993, Microstructures in feldspars from a major crustal thrust zone: The Grenville Front, Ontario, Canada: Journal of Structural Geology, v. 15, no. 1, p. 21–36, doi:10.1016/0191-8141(93)90076-M.

Rahn, M.K., Brandon, M.T., Batt, G.E., and Garver, J.I., 2004, A zero-damage model for fission-track annealing in zircon: The American Mineralogist, v. 89, no. 4, p. 473–484.

Raine, J.I., 1984, Outline of a palynological zonation of Cretaceous to Paleogene terrestrial sediments in West Coast region, South Island, New Zealand: New Zealand Geological Survey, Report NZGS 109, 82 p.

Rattenbury, M.S., Cooper, R.A., and Johnston, M.R., 1998, Geology of the Nelson area: Institute of Geological & Nuclear Science 1:250 000 geological map 9. 1 sheet + 67 p: Institute of Geological & Nuclear Sciences Limited.

Reiners, P.W., and Brandon, M.T., 2006, Using thermochronology to understand orogenic erosion: Annual Review of Earth and Planetary Sciences, v. 34, no. 1, p. 419–466, doi:10.1146/annurev.earth.34.031405.125202.

Reynolds, S.J., and Rehrig, W.A., 1980, Mid-Tertiary plutonism and mylonitization, South Mountains, central Arizona, *in* Crittenden, M.D., Coney, P.J., and Davis, G.H., eds., Cordilleran Metamorphic Core Complexes: Geological Society of America, Memoirs 153, p. 159–175.

Ring, U., and Bernet, M., 2010, Fission-track analysis unravels the denudation history of the Bonar Range in the footwall of the Alpine Fault, South Island, New Zealand: Geological Magazine, v. FirstView, p. 1–13.

Sagar, M.W., and Palin, M., 2011, Emplacement, metamorphism, deformation and affiliation of mid-Cretaceous orthogneiss from the Paparoa Metamorphic Core Complex lower-plate, Charleston, New Zealand: New Zealand Journal of Geology and Geophysics, v. 54, no. 3, p. 273–289, doi:10.1080/00288306.2011.562904.

Sambridge, M.S., and Compston, W., 1994, Mixture modeling of multi-component data sets with application to ion-probe zircon ages: Earth and Planetary Science Letters, v. 128, no. 3-4, p. 373–390, doi:10.1016/0012-821X(94)90157-0.

Seward, D., 1989, Cenozoic basin histories determined by fission-track dating of basement granites, South Island, New Zealand: Chemical Geology. Isotope Geoscience Section, v. 79, no. 1, p. 31–48, doi:10.1016/0168-9622(89)90005-5.

Seward, D., and White, P.J., 1992, Evolution and eversion of a tertiary sedimentary basin, Paparoa Range, West Coast, South Island, New Zealand: Evidence from fission-track dating: New Zealand Journal of Geology and Geophysics, v. 35, no. 3, p. 265–271, doi:10.1080/00288306.1992.9514520.

Siddoway, C.S., 2008, Tectonics of the West Antarctic Rift System: New Light on the History and Dynamics of Distributed Intracontinental Extension (invited paper), Antarctica: A Keystone in a Changing World., *in* Proceedings of the 10th International Symposium on Atlantic Earth Sciences, Washington D.C., The National Academic Press.

Spell, T.L., McDougall, I., and Tulloch, A.J., 2000, Thermochronologic constraints on the breakup of the Pacific Gondwana margin: The Paparoa metamorphic core complex, South Island, New Zealand: Tectonics, v. 19, no. 3, p. 433–451, doi:10.1029/1999TC900046.

Steiger, R.H., and Jäger, E., 1977, Subcommission on geochronology: Convention on the use of decay constants in geo- and cosmochronology: Earth and Planetary Science Letters, v. 36, no. 3, p. 359–362, doi:10.1016/0012-821X(77)90060-7.

Suggate, R.P., 1959, New Zealand coals. Their geological setting and its influence on their properties: New Zealand Department of Scientific and Industrial Research Bulletin no. 134, 113 p.

Tagami, T., Galbraith, R.F., Yamada, R., and Laslett, G.M., 1998, Revised annealing kinetics of fission tracks in zircon and geological implications, *in* Van den haute, P., and De Corte, F., eds., Advances in Fission-Track Geochronology: New York, Springer, p. 99–112.

Teyssier, C., Ferré, E.C., Whitney, D.L., Norlander, B., Vanderhaeghe, O., and Parkinson, D., 2005, Flow of partially molten crust and origin of detachments during collapse of the Cordilleran Orogen, *in* Bruhn, D., and Burlini, L., High-Strain Zones: Structure and Physical Properties: Geological Society, London, Special Publication 245, p. 39–64.

Thomson, S.N., and Ring, U., 2006, Thermochronologic evaluation of postcollision extension in the Anatolide orogen, western Turkey: Tectonics, v. 25, no. 3, TC3005, doi:10.1029/2005TC001833.

Tulloch, A.J., 1988, Batholiths, plutons and suites: Nomenclature for the granitoid rocks of Westland-Nelson: New Zealand Journal of Geology and Geophysics, v. 31, p. 505–509, doi:10.1080/00288306.1988.10422147.

Tulloch, A.J., and Kimbrough, D.L., 1989, The Paparoa Metamorphic Core Complex, New Zealand: Cretaceous extension associated with fragmeotation of the Pacific margin of Gondwana: Tectonics, v. 8, no. 6, p. 1217–1234, doi:10.1029/TC008i006p01217.

Tulloch, A.J., and Palmer, K., 1990, Tectonic implications of the granite cobbles from the mid-Cretaceous Pororari Group, southwest Nelson, New Zealand: New Zealand Journal of Geology and Geophysics, v. 33, p. 205–217, doi:10.1080/00288306.1990.10425679.

Tulloch, A.J., Ramezani, J., Mortimer, N., Mortensen, J., Van den Bogaard, P., and Maas, R., 2009, Cretaceous felsic volcanism in New Zealand and Lord Howe Rise (Zealandia) as a precursor to final Gondwana break-up, *in* Ring, U., and Wernicke, B., eds., Extending a continent: architecture, rheology and heat budget: Geological Society Special Paper 321, p. 89–118.

Villa, I.M., 2010, Disequilibrium textures versus equilibrium modelling: geochronology at the crossroads: Geological Society of London, Special Publication 332, no. 1, p. 1–15, doi:10.1144/SP332.1.

Waight, T.E., Weaver, S.D., and Muir, R.J., 1998, Mid-Cretaceous granitic magmatism during the transition from subduction to extension in southern New Zealand: a chemical and tectonic synthesis: Lithos, v. 45, no. 1-4, p. 469–482, doi:10.1016/S0024-4937(98)00045-0.

Wellman, H., 1955, New Zealand quaternary tectonics: Geologische Rundschau, v. 43, no. 1, p. 248–257, doi:10.1007/BF01764108.

White, P.J., 1994, Thermobarometry of the Charleston Metamorphic Group and implications for the evolution of the Paparoa Metamorphic Core Complex, New Zealand: New Zealand Journal of Geology and Geophysics, v. 37, no. 2, p. 201–209, doi:10.1080/00288306.1994.9514615.

Zoback, M.L., Anderson, R.E., and Thompson, G.A., 1981, Cainozoic Evolution of the State of Stress and Style of Tectonism of the Basin and Range Province of the Western United States: Philosophical Transactions of the Royal Society of London. Series A: Mathematical and Physical Sciences, v. 300, no. 1454, p. 407–434, doi:10.1098/rsta.1981.0073.

MANUSCRIPT RECEIVED 6 NOVEMBER 2013
REVISED MANUSCRIPT RECEIVED 6 FEBRUARY 2014
MANUSCRIPT ACCEPTED 21 MARCH 2014

Printed in the USA